[redacted]

# Free and mixed convection boundary-layer flow of non-Newtonian fluids

## 10.1 Introduction

It is well known that most fluids which are encountered in chemical and allied processing applications do not adhere to the classical Newtonian viscosity postulate and are accordingly known as non-Newtonian fluids. One particular class of materials which are of considerable practical importance is that in which the viscosity depends on the shear stress or on the flow rate. Most slurries, suspensions and dispersions, polymer solutions, melts and solutions of naturally occurring high-molecular-weight, synthetic polymers, pharmaceutical formulations, cosmetics and toiletries, paints, biological fluids, synthetic lubricants and foodstuffs, exhibit complex rheological behaviour which is not experienced when handling ordinary low-molecular-weight Newtonian fluids such as air, water, silicon oils, etc. Due to the importance of the applications of non-Newtonian fluids for the design of equipment and in industrial processing, considerable efforts have been directed towards the analysis and understanding of such fluids. Non-Newtonian fluid behaviour has been the subject of recent books by Astarita and Marrucci (1974), Schowalter (1978), Crochet *et al.* (1984), Tanner (1985), Bird *et al.* (1987) and Siginer *et al.* (1999). Further, a fairly large body of fundamental research on non-Newtonian fluid flow can also be found in a number of excellent review articles, e.g. Cho and Hartnett (1982), Shenoy and Mashelkar (1982), Crochet and Walters (1983), Shenoy (1986), Irvine, Jr. and Karni (1987), Andersson and Irgens (1990) and Ghosh and Upadhyay (1994).

Real fluids and their mathematical models are classified into the following three types, see Andersson and Irgens (1990):

(i) Time-independent fluids for which the properties are independent of time;

(ii) Time-dependent fluids for which the properties change with time as the fluid is deformed;

(iii) Viscoelastic fluids which exhibit both viscous and elastic behaviour, e.g. elastic recovery after deformation, and stress relaxation.

The time-independent fluids may be subdivided into four types, depending on the general nature of the viscosity function, as follows:

$$\eta(\dot{\gamma}) = \frac{\tau(\dot{\gamma})}{\dot{\gamma}} \tag{10.1}$$

where $\dot{\gamma}$ is the shear rate and $\tau(\dot{\gamma})$ is the shear stress. The four types are as follows:

(i) Viscoplastic fluids (e.g. Bingham-fluids);

(ii) Pseudo-plastic or shear thinning fluids;

(iii) Dilatant or shear thickening fluids;

(iv) Newtonian fluids.

In dealing with the complexities of non-Newtonian fluid flows, methods that allow the description, interpretation and correlation of fluids properties are required. A number of mathematical models and techniques have been proposed to describe the rheological behaviour of such fluids, see for example Rosen (1979) and Bird *et al.* (1987). Some empirical models have been found to correlate the viscosity data adequately for various types of material through the use of a limited number of meaningful parameters. Despite the trend to develop constitutive theories through the application of continuum theories, simple models have been developed which describe the non-Newtonian behaviour of fluids which have useful applications in industry, see for example Cramer and Marchello (1968). Ideally, a simple model should give an accurate fit with all the available data and have a minimum number of independent constants which can be easily evaluated and they have some physical basis.

Such a model which has been most widely used for non-Newtonian fluids, and is frequently encountered in chemical engineering processes, is the empirical Ostwald-de Waele model, or the so-called power-law model, defined as follows:

$$\tau(\dot{\gamma}) = \mu_0 |\dot{\gamma}|^{n-1} \dot{\gamma} \tag{10.2}$$

where $\mu_0$ and $n$ are material parameters, $\mu_0$ is called the consistency coefficient and $n$ is the power-law index with $n$ being non-dimensional and the dimension of $\mu_0$ depends on the value of $n$. The quantity $\mu_0$ is not the viscosity in a classical sense unless $n$ is unity. The parameter $n$ is an important index to subdivide fluids

into pseudo-plastic fluids $n < 1$ (most macromolecular fluids are of this kind with $0.2 < n < 0.6$, see Bird *et al.*, 1987) and dilatant fluids $n > 1$. Clearly, the power-law model described by Equation (10.2) reduces to the Newtonian model when $n = 1$ and then the consistency coefficient $\mu_0$ is the dynamic viscosity. Details of this class of fluids can be found in the review articles by Metzner (1965) and Andersson and Irgens (1990).

Other important non-Newtonian fluids are those fluids which contain certain additives and some naturally occurring fluids such as animal blood. Physically these fluids may form suitable non-Newtonian fluid models which can be used to analyse the behaviour of exotic lubricants, colloidal suspensions, liquid crystals, etc. A mathematical model for the description of such fluids, which exhibit certain microscopic effects arising from the local structure and microrotations of the fluid elements is that of a microfluid, first introduced by Eringen (1966). As this model is not easily amenable to theoretical treatment, a subclass, known as micropolar fluids, was further proposed by Eringen (1972) and such fluids exhibit the micro-rotational inertia. They can support couple stresses and body couples only, and may represents fluids consisting of bar-like or sphere-like elements. The theory of micropolar fluids has generated a considerable amount of interest and many flow problems have been studied, see for example Ariman *et al.* (1973), Pop *et al.* (1998c) and Rees and Pop (1998) for detailed references.

However, more theoretical and experimental work is still required in the area of convective flow of non-Newtonian fluids for both power-law and micropolar fluids.

## 10.2 Free convection boundary-layer flow of power-law fluids over a vertical flat plate

This problem has been studied rather extensively since the pioneering work of Acrivos (1960). Because most non-Newtonian fluids are highly viscous and have a large Prandtl number, Acrivos (1960) presented the concept of an asymptotic boundary-layer for power-law fluids with large Prandtl numbers. He was the first to obtain similarity solutions for free convection boundary-layer of power-law fluids along a vertical flat plate. Subsequently, a large number of research papers which deal with integral, numerical and experimental methods to yield solutions of a vertical plate free convection boundary-layer with uniform wall temperature and uniform surface heat flux conditions have been published. Tien (1967) obtained an approximate integral solution for a vertical flat plate with constant surface temperature assuming a velocity profile that does not attain a zero value at a well-defined momentum boundary-layer thickness. This is a result of not using the appropriate boundary and compatibility conditions when making the choice of the velocity and temperature profiles. The average Nusselt number predicted by Tien (1967) is, however, correct as can be seen from Table 10.1 showing the comparison of the results

Table 10.1: *Comparison of the modified average Nusselt number,* $\frac{\overline{Nu}}{Ra^{\frac{1}{3n+1}}}$, *for* $Pr_x \to \infty$.

| $n$ | Acrivos (1960) | Tien (1967) | Shenoy and Ulbrecht (1979) | Kawase and Ulbrecht (1984) | Huang and Chen (1990) |
|---|---|---|---|---|---|
| 0.5 | 0.63 | 0.6098 | 0.5957 | 0.6275 | 0.6105 |
| 1.0 | 0.67 | 0.6838 | 0.6775 | 0.6700 | 0.6701 |
| 1.5 | 0.71 | 0.7229 | 0.7194 | 0.6960 | 0.7012 |

of the four theoretical approaches. Emery *et al.* (1970) have experimentally investigated the free convection boundary-layer of power-law fluids and they have also used a composite fluid model to obtain numerical solutions. Shulman *et al.* (1976) have solved this problem analytically using the method of matched asymptotic expansions. Kawase and Ulbrecht (1984) have employed an integral method, assuming a very thin thermal boundary-layer and using a velocity profile taken from the forced convection analysis and hence the energy and momentum equations become decoupled. All these studies were based on the assumption of an infinite value of the Prandtl number and this is, in general, a good approximation, e.g. 0.5% carboxymethylcellulose water solution has $Pr = 85 - 500$; 0.05% carbopal solution 934 has $Pr = 65 - 90$. If we take into account the finiteness of the Prandtl number then the governing boundary-layer equations for the free convection flow along a vertical plate which is immersed in power-law fluids are in general non-similar. Wang and Kleinstreuer (1987) and Huang *et al.* (1989) have employed the Keller-box method to numerically solve the coupled system of non-similar equations for this problem. We shall present here some of the results obtained by Huang and Chen (1990) for the problem of free convection boundary-layer flow over an isothermal vertical flat plate in a non-Newtonian power-law fluid using the method of local similarity.

Consider a vertical flat plate which is at a constant temperature $T_w$ and it is placed in a non-Newtonian power-law fluid of ambient temperature $T_\infty$ ($< T_w$) and pressure $p_\infty$, which obeys the Ostwald-de Waele power-law model, see Andersson and Irgens (1990), namely

$$\tau_{ij} = 2\mu_0 \left(2e_{ij}e_{ji}\right)^{\frac{n-1}{2}} \tag{10.3}$$

where $\tau_{ij}$ is the stress tensor and

$$e_{ij} = \frac{1}{2}\left(\frac{\partial u_i}{\partial x_j} + \frac{\partial u_j}{\partial x_i}\right) \tag{10.4}$$

denotes the strain rate. The governing equations for the steady free convection of non-Newtonian power-law fluids stem from those which are commonly used for

analysing the continuity, momentum and energy equations and they are given by

$$\frac{\partial u}{\partial x}+\frac{\partial v}{\partial y}=0 \tag{10.5}$$

$$u\frac{\partial u}{\partial x}+v\frac{\partial u}{\partial y}=-\frac{1}{\rho}\frac{\partial p}{\partial x}+\frac{\mu_0}{\rho}\left\{2\frac{\partial}{\partial x}\left(J\frac{\partial u}{\partial x}\right)+\frac{\partial}{\partial y}\left[J\left(\frac{\partial u}{\partial y}+\frac{\partial v}{\partial x}\right)\right]\right\}+g\beta\left(T-T_\infty\right) \tag{10.6}$$

$$u\frac{\partial v}{\partial x}+v\frac{\partial v}{\partial y}=-\frac{1}{\rho}\frac{\partial p}{\partial y}+\frac{\mu_0}{\rho}\left\{\frac{\partial}{\partial x}\left[J\left(\frac{\partial u}{\partial y}+\frac{\partial v}{\partial x}\right)\right]+2\frac{\partial}{\partial y}\left(J\frac{\partial v}{\partial y}\right)\right\} \tag{10.7}$$

$$u\frac{\partial T}{\partial x}+v\frac{\partial T}{\partial y}=\alpha_f\left(\frac{\partial^2 T}{\partial x^2}+\frac{\partial^2 T}{\partial y^2}\right) \tag{10.8}$$

where $J$ is the Ostwald-de Waele power-law model parameter which, from Equations (10.3) and (10.4), is given by

$$J=\left[2\left(\frac{\partial u}{\partial x}\right)^2+2\left(\frac{\partial v}{\partial y}\right)^2+\left(\frac{\partial u}{\partial y}+\frac{\partial v}{\partial x}\right)^2\right]^{\frac{n-1}{2}} \tag{10.9}$$

Equations (10.5) – (10.8) can be transformed further by using the following non-dimensional variables

$$\begin{gathered}\widehat{x}=\tfrac{x}{l},\quad \widehat{y}=\tfrac{y}{l},\quad \widehat{u}=\tfrac{u}{U_c},\quad \widehat{v}=\tfrac{v}{U_c}\\ \widehat{p}=\tfrac{p-p_\infty}{\rho U_c^2},\quad \widehat{\theta}=\tfrac{T-T_\infty}{\Delta T},\quad U_c=(g\beta\Delta T l)^{\frac{1}{2}}\end{gathered} \tag{10.10}$$

On substituting the variables (10.10) into Equations (10.5) – (10.8) we obtain

$$\frac{\partial \widehat{u}}{\partial \widehat{x}}+\frac{\partial \widehat{v}}{\partial \widehat{y}}=0 \tag{10.11}$$

$$\widehat{u}\frac{\partial \widehat{u}}{\partial \widehat{x}}+\widehat{v}\frac{\partial \widehat{u}}{\partial \widehat{y}}=-\frac{\partial \widehat{p}}{\partial \widehat{x}}+Gr^{-\frac{1}{2}}\left\{\frac{\partial}{\partial \widehat{x}}\left(\widehat{J}\frac{\partial \widehat{u}}{\partial \widehat{x}}\right)+\frac{\partial}{\partial \widehat{y}}\left[\widehat{J}\left(\frac{\partial \widehat{u}}{\partial \widehat{y}}+\frac{\partial \widehat{v}}{\partial \widehat{x}}\right)\right]\right\}+\widehat{\theta} \tag{10.12}$$

$$\widehat{u}\frac{\partial \widehat{v}}{\partial \widehat{x}}+\widehat{v}\frac{\partial \widehat{v}}{\partial \widehat{y}}=-\frac{\partial \widehat{p}}{\partial \widehat{y}}+Gr^{-\frac{1}{2}}\left\{\frac{\partial}{\partial \widehat{x}}\left[\widehat{J}\left(\frac{\partial \widehat{u}}{\partial \widehat{y}}+\frac{\partial \widehat{v}}{\partial \widehat{x}}\right)\right]+2\frac{\partial}{\partial \widehat{y}}\left(\widehat{J}\frac{\partial \widehat{v}}{\partial \widehat{y}}\right)\right\} \tag{10.13}$$

$$\widehat{u}\frac{\partial \widehat{\theta}}{\partial \widehat{x}}+\widehat{v}\frac{\partial \widehat{\theta}}{\partial \widehat{y}}=\frac{1}{Pr}Gr^{-\frac{1}{n+1}}\left(\frac{\partial^2 \widehat{\theta}}{\partial \widehat{x}^2}+\frac{\partial^2 \widehat{\theta}}{\partial \widehat{y}^2}\right) \tag{10.14}$$

where $\widehat{J}=U_c^{1-n}l^{n-1}J$ and $Gr$ and $Pr$ are the modified Grashof and Prandtl numbers which are defined as

$$Gr=\frac{(g\beta\Delta T)^{2-n}\,l^{2+n}}{\left(\frac{\mu_0}{\rho}\right)^2},\qquad Pr=\frac{1}{\alpha_f}\left(\frac{\mu_0}{\rho}\right)^{\frac{2}{n+1}}(g\beta\Delta T)^{\frac{3(n-1)}{2(n+1)}}\,l^{\frac{n-1}{2(n+1)}} \tag{10.15}$$

Next we introduce the boundary-layer variables

$$\widetilde{x} = \widehat{x}, \quad \widetilde{y} = Gr^{\frac{1}{2(n+1)}}\widehat{y}, \quad \widetilde{u} = \widehat{u}, \quad \widetilde{v} = Gr^{\frac{1}{2(n+1)}}\widehat{v}, \quad \widetilde{p} = \widehat{p}, \quad \widetilde{\theta} = \widehat{\theta} \tag{10.16}$$

into Equations (10.11) - (10.14) and neglect terms which are asymptotically small compared with the retained terms as $Gr \to \infty$. We then obtain, in dimensional variables, the boundary-layer equations for the free convection flow over a vertical flat plate which is immersed in a non-Newtonian power-law fluid of the form:

$$\frac{\partial u}{\partial x} + \frac{\partial v}{\partial y} = 0 \tag{10.17}$$

$$u\frac{\partial u}{\partial x} + v\frac{\partial u}{\partial y} = \frac{\mu_0}{\rho}\frac{\partial}{\partial y}\left(\left|\frac{\partial u}{\partial y}\right|^{n-1}\frac{\partial u}{\partial y}\right) + g\beta\left(T - T_\infty\right) \tag{10.18}$$

$$u\frac{\partial T}{\partial x} + v\frac{\partial T}{\partial y} = \alpha_f\frac{\partial^2 T}{\partial y^2} \tag{10.19}$$

and these equations have to be solved subject to the boundary conditions

$$\begin{array}{llll} u = 0, & v = 0, & T = T_w & \text{on} \quad y = 0, \quad x \geqslant 0 \\ u \to 0, & T \to T_\infty & & \text{as} \quad y \to \infty, \quad x \geqslant 0 \end{array} \tag{10.20}$$

Following Huang and Chen (1990), we look for local similarity solutions of Equations (10.17) - (10.20) of the form

$$\eta = \frac{y}{\delta_T(x)}, \quad f(\eta) = \frac{\psi}{\frac{\alpha_f x}{\delta_T(x)}}, \quad \theta(\eta) = \frac{T - T_\infty}{\Delta T} \tag{10.21}$$

where $\psi$ is the stream function, defined by Equation (1.18), the thermal boundary-layer thickness $\delta_T(x)$ is written as

$$\delta_T(x) = \frac{x}{Ra_x^{\frac{1}{3n+1}}} \tag{10.22}$$

and the modified local Rayleigh number is defined as

$$Ra_x = \frac{\left(\frac{\rho}{\mu_0}\right)g\beta\Delta T x^{2n+1}}{\alpha_f^n} \tag{10.23}$$

On substituting Equation (10.21) into Equations (10.18) and (10.19) we obtain the following set of ordinary differential equations

$$Pr_x^{\frac{2(n+1)}{3n+1}}\left[\theta + \left(\left|f''\right|^{n-1}f''\right)'\right] + \frac{2n+1}{3n+1}ff'' - \frac{n+1}{3n+1}f'^2 = 0 \tag{10.24}$$

$$\theta'' + \frac{2n+1}{3n+1}f\theta' = 0 \tag{10.25}$$

which have to be solved subject to the boundary conditions (10.20) which become

$$\begin{array}{c} f(0) = 0, \quad f'(0) = 0, \quad \theta(0) = 1 \\ f' \to 0, \quad \theta \to 0 \quad \text{as} \quad \eta \to \infty \end{array} \tag{10.26}$$

where $Pr_x$ is the modified local Prandtl number and is defined as

$$Pr_x = \frac{1}{\alpha_f} \left( \frac{\mu_0}{\rho} \right)^{\frac{2}{n+1}} x^{\frac{n-1}{2(n+1)}} (g\beta\Delta T)^{\frac{3(n-1)}{2(n+1)}} \tag{10.27}$$

Finally, the modified local and average Nusselt numbers are given by

$$\frac{Nu}{Ra_x^{\frac{1}{3n+1}}} = -\theta'(0), \qquad \frac{\overline{Nu}}{Ra^{\frac{1}{3n+1}}} = \frac{3n+1}{2n+1} \left[ -\theta'(0) \right] \tag{10.28}$$

where $Ra$ is the modified Rayleigh number based on the length scale $l$.

Equations (10.24) – (10.26) have been solved numerically by Huang and Chen (1990) using a finite-difference method in combination with a cubic spline interpolation procedure proposed by Lee *et al.* (1986). This solution method has been found to yield rapid convergence and results of high accuracy. The method is very effective in dealing with the stiff Equation (10.24) which becomes

$$\theta + \left( |f''|^{n-1} f'' \right)' = 0 \tag{10.29a}$$

when $Pr_x \gg 1$. Equation (10.29a) has to be solved subject to the boundary conditions

$$f(0) = 0, \quad f'(0) = 0, \quad f''(\infty) = 0 \tag{10.29b}$$

and therefore the numerical solutions are independent of $Pr_x$.

Typical reduced fluid velocity and temperature profiles are shown in Figure 10.1 for the flow index $n = 0.5$, 1 (Newtonian fluids) and 1.5, when $Pr_x = 1$, 10, 100 and 1000. It is seen that the fluid velocity profiles are strongly sensitive to the modified local Prandtl number and the fluid flow index, while the temperature profiles are clearly not influenced.

The effect of the modified local Prandtl number on the modified local Nusselt number, as obtained by Huang and Chen (1990), is shown (by full lines) in Figure 10.2 and the integral solutions of Shenoy and Ulbrecht (1979), and Kawase and Ulbrecht (1984) are also included in this figure. It is seen that the modified local Nusselt number increases as $Pr_x$ increases for all values of $n$. It also increases monotonically as $n$ increases. In addition, for large values of $Pr_x$ ($\gtrsim 100$), the modified local Nusselt number reaches a constant value for all values of $n$ because in this case Equation (10.24) is approximated by the Equation (10.29) and thus its solution becomes independent of $Pr_x$. Further, we note from Figure 10.2 that the approximate results of Kawase and Ulbrecht (1984) compare well with the exact solution

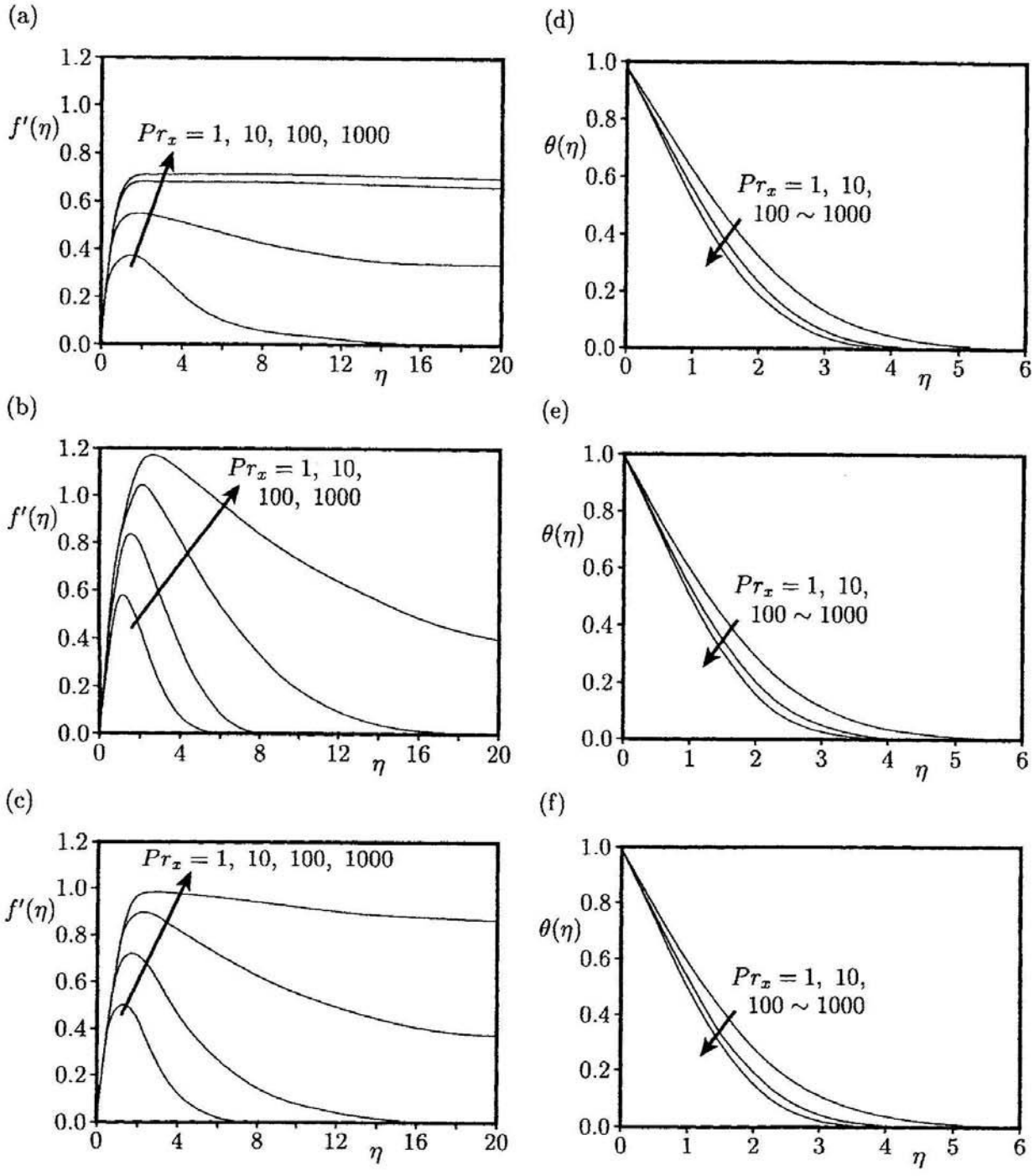


Figure 10.1: *Fluid velocity profiles, $f'(\eta)$, for (a) $n = 0.5$, (b) $n = 1$ and (c) $n = 1.5$ and temperature profiles, $\theta(\eta)$, for (d) $n = 0.5$, (e) $n = 1$ and (f) $n = 1.5$.*

of Huang and Chen (1990) for $n > 0.9$ and very large values of $Pr_x$. However, the approximate results of Shenoy and Ulbrecht (1979) deviate from those of Huang

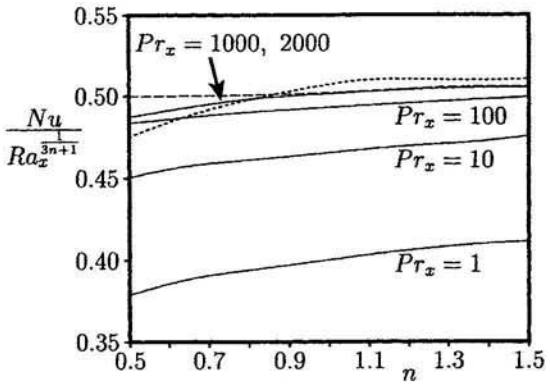


Figure 10.2: *Variation of the local Nusselt number with the power-law index n. The solutions of Huang and Chen (1990) are indicated by the solid line and the integral solutions of Shenoy and Ulbrecht (1979) and Kawase and Ulbrecht (1984) are indicated by the dotted and broken lines, respectively.*

and Chen (1990) for all values of $n$, even at large values of $Pr_x$. Consequently, we conclude that the results of Huang and Chen (1990) are reasonably good for $Pr_x$ ranging from 1 to 1000.

Finally, values of the modified average Nusselt number, $\overline{Nu}$, as defined in Equation (10.28) and those obtained by some other authors are given in Table 10.1 for $n = 0.5$, 1 and 1.5 when $Pr_x \to \infty$. It is observed that the local similarity solutions proposed by Huang and Chen (1990) give very good results for high values of the modified local Prandtl number.

## 10.3 Free convection boundary-layer flow of non-Newtonian power-law fluids over a vertical wavy surface

The prediction of the heat transfer from irregular surfaces is a topic of fundamental importance for many practical problems. Surfaces are sometimes roughened in order to enhance heat transfer, for example in flat-plate solar collectors and flat-plate condensers in refrigerators. The presence of roughness elements on a flat surface disturbs the fluid flow and hence changes the rate of heat transfer. Yao (1983) was probably the first who used the Prandtl transposition theorem, see Yao (1988), to analyse the steady free convection boundary-layer of a non-Newtonian fluid over a vertical wavy surface. A simple coordinate transformation was proposed to transform the wavy surface to a simple shape, namely that of a flat plate. The gist of the theorem is that

the flow is displaced by the irregularities on the vertical surface and the horizontal component of the fluid velocity is adjusted according to the shape of the surface. The form of the boundary-layer equations is invariant under the transformation and the surface conditions can therefore be applied on a transformed flat surface. Moulic and Yao (1989), Chiu and Chou (1993, 1994), Rees and Pop (1994a, 1994b, 1995a, 1995b), Chen *et al.* (1996), Yang *et al.* (1996), Kumari *et al.* (1996a), Kim (1997) and Pop and Na (1999) have used the transformation proposed by Yao (1983) to solve free convection problems associated with Newtonian fluids, micropolar fluids, fluid-saturated porous media and non-Newtonian power-law fluids.

Consider the steady laminar free convection of a non-Newtonian power-law fluid over a wavy vertical surface which is maintained at the constant temperature $T_w$, where $T_w > T_\infty$. The physical model and the coordinate system are shown in Figure 10.3, where $x$ and $y$ are the axial and transverse Cartesian coordinates, $a$ is the amplitude of the surface wave and $l$ is a characteristic wavelength of the surface waves. In particular, we assume that the surface profile is given by

$$y = \sigma(x) \tag{10.30}$$

where $\sigma(x)$ is an arbitrary geometric function.

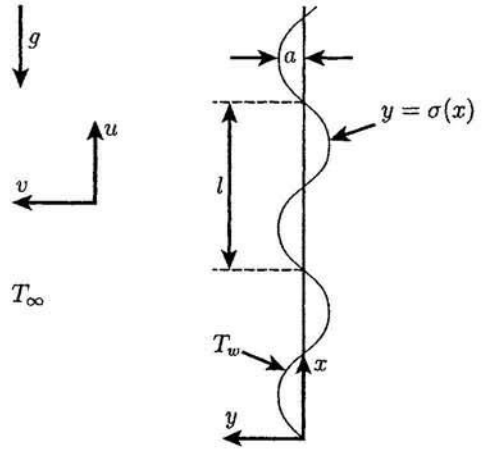


Figure 10.3: *Physical model and coordinate system.*

The governing equations for this problem, in non-dimensional form, are Equations (10.11) – (10.14) and they have to be solved subject to the boundary (non-dimensional) conditions

$$\begin{array}{llll} \widehat{u} = 0, \quad \widehat{v} = 0, \quad \theta = 1 & \text{on} & \widehat{y} = \widehat{\sigma}\,(\widehat{x}), & \widehat{x} \geqslant 0 \\ \widehat{u} \to 0, \quad \widehat{v} \to 0, \quad \widehat{p} \to 0, \quad \theta \to 0 & \text{as} & \widehat{y} \to \infty, & \widehat{x} \geqslant 0 \end{array} \tag{10.31}$$

where $\widehat{\sigma}(\widehat{x}) = \frac{\sigma(x)}{l}$. We now assume that the modified Grashof number is so large that free convection takes place within a boundary-layer, whose cross-section width is substantially smaller than the amplitude $\widehat{a}$ $(= \frac{a}{l})$ of the waves on the surface. Thus, invoking the boundary-layer scalings given by the transformations

$$\widetilde{x} = \widehat{x}, \quad \widetilde{y} = (\widehat{y} - \widehat{\sigma})\, Gr^{\frac{1}{2(n+1)}}, \quad \widetilde{u} = \widehat{u}, \quad \widetilde{v} = (\widehat{v} - \widetilde{\sigma}_x \widehat{u})\, Gr^{\frac{1}{2(n+1)}}, \quad \widetilde{p} = \widehat{p}, \quad \widetilde{\sigma} = \widehat{\sigma} \tag{10.32}$$

where $\widetilde{\sigma}_x = \frac{\mathrm{d}\widetilde{\sigma}}{\mathrm{d}\widetilde{x}}$, Equations (10.11) – (10.14) reduce, to leading order as $Gr \to \infty$, to the following boundary-layer equations:

$$\frac{\partial \widetilde{u}}{\partial \widetilde{x}} + \frac{\partial \widetilde{v}}{\partial \widetilde{y}} = 0 \tag{10.33}$$

$$\widetilde{u}\frac{\partial \widetilde{u}}{\partial \widetilde{x}} + \widetilde{v}\frac{\partial \widetilde{u}}{\partial \widetilde{y}} = -\frac{\partial \widetilde{p}}{\partial \widetilde{x}} + \widetilde{\sigma}_x Gr^{\frac{1}{2(n+1)}} \frac{\partial \widetilde{p}}{\partial \widetilde{y}} + \left(1 + \widetilde{\sigma}_x^2\right)^n \frac{\partial}{\partial \widetilde{y}} \left( \left| \frac{\partial \widetilde{u}}{\partial \widetilde{y}} \right|^{n-1} \frac{\partial \widetilde{u}}{\partial \widetilde{y}} \right) + \theta \tag{10.34}$$

$$\widetilde{\sigma}_{xx}\widetilde{u}^2 + \widetilde{\sigma}_x \left( \widetilde{u}\frac{\partial \widetilde{u}}{\partial \widetilde{x}} + \widetilde{v}\frac{\partial \widetilde{u}}{\partial \widetilde{y}} \right) = -Gr^{\frac{1}{2(n+1)}} \frac{\partial \widetilde{p}}{\partial \widetilde{y}} + \widetilde{\sigma}_x \left(1 + \widetilde{\sigma}_x^2\right)^n \frac{\partial}{\partial \widetilde{y}} \left( \left| \frac{\partial \widetilde{u}}{\partial \widetilde{y}} \right|^{n-1} \frac{\partial \widetilde{u}}{\partial \widetilde{y}} \right) \tag{10.35}$$

$$\widetilde{u}\frac{\partial \theta}{\partial \widetilde{x}} + \widetilde{v}\frac{\partial \theta}{\partial \widetilde{y}} = \frac{1 + \widetilde{\sigma}_x^2}{Pr} \frac{\partial^2 \theta}{\partial \widetilde{y}^2} \tag{10.36}$$

and the boundary conditions (10.31) become

$$\begin{aligned} \widetilde{u} = 0, \quad \widetilde{v} = 0, \quad \theta = 1 \quad &\text{on} \quad \widetilde{y} = 0, \quad \widetilde{x} \geqslant 0 \\ \widetilde{u} \to 0, \quad \theta \to 0 \quad &\text{as} \quad \widetilde{y} \to \infty, \quad \widetilde{x} \geqslant 0 \end{aligned} \tag{10.37}$$

It is noted from these boundary conditions that the new variable $\widetilde{y}$, defined in Equation (10.32), transforms the wavy surface into a flat surface. Also it should be noted that this analysis is valid only within the framework of boundary-layer theory with $\widehat{y} = \mathbf{O}\left(Gr^{-\frac{1}{2(n+1)}}\right)$ and $\widehat{a} = \mathbf{O}\left(Gr^{-\frac{1}{2(n+1)}}\right)$ as $Gr \to \infty$, as obtained from Equations (10.30) and (10.32). Further, Equation (10.35) indicates that $\frac{\partial \widetilde{p}}{\partial \widetilde{y}} = \mathbf{O}\left(Gr^{-\frac{1}{2(n+1)}}\right)$, which implies that the lowest order pressure gradient along the $\widetilde{x}$ direction is determined from the inviscid (outer) flow solution. However, for the present problem this gives $\frac{\partial \widetilde{p}}{\partial \widetilde{x}} = 0$. In order to eliminate the term $Gr^{\frac{1}{2(n+1)}} \frac{\partial \widetilde{p}}{\partial \widetilde{y}}$ from Equations (10.34) and (10.35), we multiply Equation (10.35) by $\widetilde{\sigma}_x$ and the resulting equation is added to Equation (10.34). After a little algebra, we obtain

$$\widetilde{u}\frac{\partial \widetilde{u}}{\partial \widetilde{x}} + \widetilde{v}\frac{\partial \widetilde{u}}{\partial \widetilde{y}} + \frac{\widetilde{\sigma}_x \widetilde{\sigma}_{xx}}{1 + \widetilde{\sigma}_x^2}\widetilde{u}^2 = \left(1 + \widetilde{\sigma}_x^2\right)^n \frac{\partial}{\partial \widetilde{y}} \left( \left| \frac{\partial \widetilde{u}}{\partial \widetilde{y}} \right|^{n-1} \frac{\partial \widetilde{u}}{\partial \widetilde{y}} \right) + \frac{\theta}{1 + \widetilde{\sigma}_x^2} \tag{10.38}$$

Equations (10.33), (10.36) and (10.38), along with the boundary conditions (10.37), form the basic equations for the problem of free convection of a non-Newtonian power-law fluid along a vertical wavy surface. These equations can

be solved numerically using the Keller-box method as described by Kumari *et al.* (1996a) for a wavy vertical surface which is subject to a constant heat flux rate. However, Kim (1997) has solved Equations (10.33), (10.36) and (10.38), along with the boundary conditions (10.37), using the finite volume method as proposed by Patankar (1980). In order to do this Kim (1997) introduced the parabolic coordinates

$$X = \widetilde{x}, \quad Y = \frac{\widetilde{y}}{[2(n+1)\widetilde{x}]^{\frac{1}{2(n+1)}}}, \quad U = \frac{\widetilde{u}}{[2(n+1)\widetilde{x}]^{\frac{1}{2n}}}, \quad V = [2(n+1)\widetilde{x}]^{\frac{1}{2(n+1)}}\,\widetilde{v} \tag{10.39}$$

so that Equations (10.33), (10.36) and (10.38) become

$$\frac{n+1}{n}U + [2(n+1)X]\frac{\partial U}{\partial X} - Y[2(n+1)X]^{\frac{(n-1)(2n+1)}{2n(n+1)}}\frac{\partial V}{\partial Y} = 0 \tag{10.40}$$

$$[2(n+1)X]^{\frac{1}{n}}U\frac{\partial U}{\partial X} + \left\{[2(n+1)X]^{\frac{1-n}{2n(n+1)}} - [2(n+1)X]^{\frac{1-n}{n}}YU\right\}\frac{\partial U}{\partial Y} + \left\{\frac{n+1}{n}[2(n+1)X]^{\frac{1-n}{n}} + \frac{\widetilde{\sigma}_x\widetilde{\sigma}_{xx}[2(n+1)X]^{\frac{1}{n}}}{1+\widetilde{\sigma}_x^2}\right\}U^2 = (1+\widetilde{\sigma}_x^2)^n\frac{\partial}{\partial Y}\left(\left|\frac{\partial U}{\partial Y}\right|^{n-1}\frac{\partial U}{\partial Y}\right) + \frac{\theta}{1+\widetilde{\sigma}_x^2} \tag{10.41}$$

$$[2(n+1)X]^{\frac{3n+1}{2n(n+1)}}U\frac{\partial\theta}{\partial X} + \left\{V - [2(n+1)X]^{\frac{(1-n)(1+2n)}{2n(n+1)}}YU\right\}\frac{\partial\theta}{\partial Y} = \frac{1+\widetilde{\sigma}_x^2}{Pr}\frac{\partial^2\theta}{\partial Y^2} \tag{10.42}$$

which have to be solved subject to the boundary conditions

$$\begin{aligned} U = 0, \quad V = 0, \quad \theta = 1 \quad &\text{on} \quad Y = 0, \quad X \geqslant 0 \\ U \to 0, \quad \theta \to 0 \quad &\text{as} \quad Y \to \infty, \quad X \geqslant 0 \end{aligned} \tag{10.43}$$

The local heat transfer coefficient may be determined from the expression

$$q_w = -k_f\,\boldsymbol{n}\cdot\nabla T \tag{10.44}$$

where

$$\boldsymbol{n} = \left(-\frac{\widetilde{\sigma}_x}{(1+\widetilde{\sigma}_x^2)^{\frac{1}{2}}}, \frac{1}{(1+\widetilde{\sigma}_x^2)^{\frac{1}{2}}}\right) \tag{10.45}$$

is the unit vector normal to the wavy surface. The local Nusselt number can then be expressed as follows:

$$Nu\left(\frac{2(n+1)X}{Gr}\right)^{\frac{1}{2(n+1)}} = -(1+\widetilde{\sigma}_x^2)^{\frac{1}{2}}\frac{\partial\theta}{\partial Y}(X,0) \tag{10.46}$$

The numerical results reported by Kim (1997) were obtained for a sinusoidal surface

$$\widetilde{\sigma}(X) = \widehat{a} \sin(2\pi X) \tag{10.47}$$

in order to show the effects of the wavy surface to the free convection flow. The full details of the numerical procedure can be found in Kim and Chen (1991) and Kim (1997) and therefore we do not repeat them here.

Kim (1997) obtained the non-dimensional axial fluid velocity, $U$, and the temperature, $\theta$, profiles for $Pr = 10$, $\widehat{a} = 0.1$, $n = 0.8$ (pseudoplastic fluids), $n = 1$ (Newtonian fluids) and $n = 1.2$ (dilatant fluids). He found that the maximum value of $U$ increases, but the boundary-layer thickness becomes thinner as the flow index $n$ increases. However, the thermal boundary layers of pseudoplastic fluids are thinner than those of dilatant fluids. Further, Kim (1997) investigated the axial velocity profiles for $Pr = 10$, $\widehat{a} = 0.1$ and $n = 1$ and showed that they are sinusoidal along the $X$ direction. The regular nodes along the $X$ direction being at $X = 1.5$ and 2.0, and $X = 1.75$ and 2.25, which represent the troughs and the crests of one wavy segment, respectively. The difference in the axial velocity at the crest and at the trough are almost indistinguishable but the boundary-layer around the nodes is thicker compared to that of the crests or the troughs. Further, it should be noted that the computation domain is not paralleled to the physical surface.

Figures 10.4 and 10.5 show the profiles of the local Nusselt number, given by Equation (10.46), for $Pr = 10$ and 1000 and for some values of the parameters $\widehat{a}$ and $n$. It can be seen from Figure 10.4 that for $n = 1$ the local Nusselt number for a wavy surface decreases as $\widehat{a}$ increases. This is because the buoyancy forces on an irregular surface are smaller than those on a flat plate ($\widehat{a} = 0$), except at

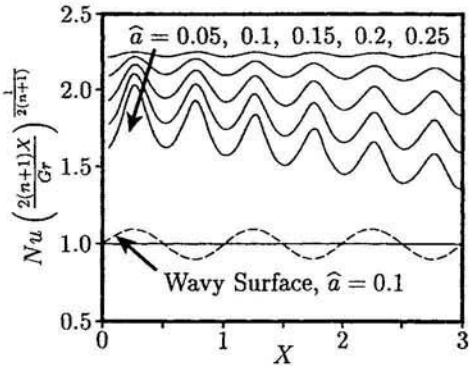


Figure 10.4: *Variation of the local Nusselt number with $X$ for $n = 1$ (Newtonian fluid) and $Pr = 10$.*

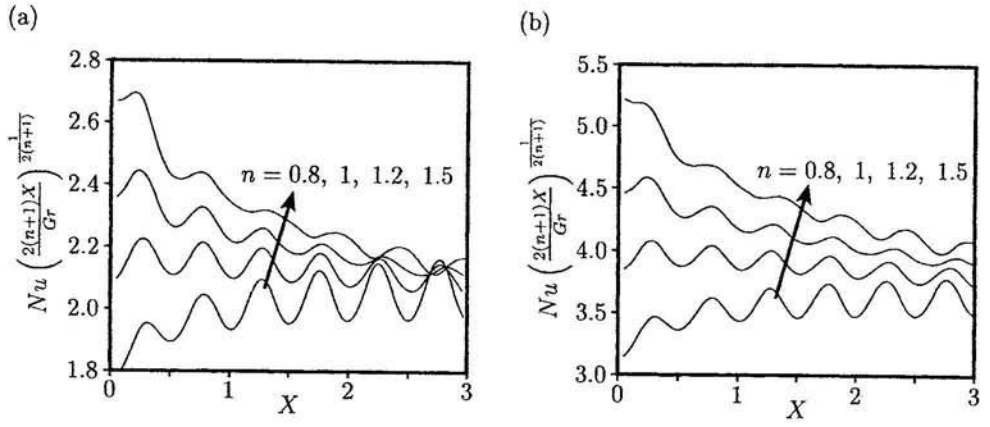


Figure 10.5: *Variation of the local Nusselt number with $X$ for $\widehat{a} = 0.1$ when (a) $Pr = 100$ and (b) $Pr = 1000$.*

the trough and crest points. On the other hand, Figure 10.5 shows that the local Nusselt number increases as $n$ increases. However, it decreases as the axial distance $X$ increases from $X = 0$ (flat plate).

## 10.4 Free convection boundary-layer wall plume in non-Newtonian power-law fluids

Consider the problem of steady, laminar free convection from a line source of heat positioned at the leading edge of an adiabatic vertical surface which is immersed in an unbounded non-Newtonian power-law fluid with the following transport properties as proposed by Shvets and Vishnevskiy (1987) and Gryglavszewski and Saljnikov (1989),

$$\tau_{ij} = -p\,\delta_{ij} + \mu_0 \left|\frac{1}{2} I_2\right|^{\frac{n-1}{2}} e_{ij}, \qquad q_s = -k_f \left|\frac{1}{2} I_2\right|^{\frac{s}{2}} |\nabla T| \tag{10.48}$$

where $\delta_{ij}$ is the unit tensor, $I_2$ is the second invariant of the strain rate tensor and $s$ is the heat transfer index. It can be shown that the boundary-layer equations in non-dimensional form for this problem are given by, see Pop *et al.* (1993b),

$$\frac{\partial u}{\partial x} + \frac{\partial v}{\partial y} = 0 \tag{10.49}$$

$$u\frac{\partial u}{\partial x} + v\frac{\partial u}{\partial y} = \frac{\partial}{\partial y}\left(\left|\frac{\partial u}{\partial y}\right|^{n-1} \frac{\partial u}{\partial y}\right) + \theta \tag{10.50}$$

$$u\frac{\partial\theta}{\partial x}+v\frac{\partial\theta}{\partial y}=\frac{1}{Pr}\frac{\partial}{\partial y}\left(\left|\frac{\partial u}{\partial y}\right|^{s}\frac{\partial\theta}{\partial y}\right) \tag{10.51}$$

which have to be solved subject to the boundary conditions

$$\left.\begin{array}{c} u=0,\quad v=0 \\ \theta=(T-T_\infty)\frac{Gr^b}{T_{\mathrm{ref}}}\quad\text{or}\quad\frac{\partial\theta}{\partial y}=0 \\ u\to 0,\quad\theta\to 0 \end{array}\right\}\quad\begin{array}{lll}\text{on} & y=0, & x\geqslant 0\\ & & \\ \text{as} & y\to\infty, & x\geqslant 0\end{array} \tag{10.52a}$$

together with the integral condition, see also Section 5.1,

$$\int_0^\infty u\theta\,\mathrm{d}y=Q \tag{10.52b}$$

where the non-dimensional variables are defined as follows:

$$\begin{gathered} x=\frac{\bar{x}}{l},\quad y=\frac{\bar{y}}{l}Gr^a,\quad u=\frac{\bar{u}}{U_c},\quad v=\frac{\bar{v}}{U_c}Gr^a,\quad\theta=\frac{T-T_\infty}{T_{\mathrm{ref}}}Gr^b \\ U_c=\left(\frac{\rho l^n Gr^{-\frac{n(n+1)}{4n+1}}}{\mu_0}\right)^{\frac{1}{n-2}},\quad Q=\frac{q_s}{\rho c_p l T_{\mathrm{ref}}}\left(\frac{\rho l^n Gr^{n-1}}{\mu_0}\right)^{\frac{1}{n-2}} \end{gathered} \tag{10.53}$$

where $a=\frac{n}{4n+1}$ and $b=\frac{6n^2-5n-2}{(4n+1)(n-2)}$. The modified Grashof and Prandtl numbers are now given by

$$Gr=\frac{g\beta T_{\mathrm{ref}}\,l^{\frac{2+n}{2-n}}}{\left(\frac{\rho}{\mu_0}\right)^{\frac{2}{n-2}}},\qquad Pr=\frac{1}{\alpha_f}l^{1+s}U_c^{1-s}Gr^{-\frac{n(2+s)}{4n+1}} \tag{10.54}$$

We now define the following variables

$$\psi=x^{\frac{2n+1}{4n+1}}f(x,\eta),\quad\theta=x^{-\frac{2n+1}{4n+1}}h(x,\eta),\quad\eta=x^{-\frac{n+1}{4n+1}}y \tag{10.55}$$

and assume that the wall temperature depends on $x$ in the following manner

$$T_w(x)=T_\infty+Gr^{-b}T_{\mathrm{ref}}\,x^{-\frac{2n+1}{4n+1}} \tag{10.56}$$

Insertion of the variables (10.55) into Equations (10.49) – (10.51) leads to

$$\left(|f''|^{n-1}f''\right)'+\frac{2n+1}{4n+1}ff''-\frac{n}{4n+1}f'^2+h=x\left(f'\frac{\partial f'}{\partial x}-f''\frac{\partial f}{\partial x}\right) \tag{10.57}$$

$$x^{\frac{n-1-s}{4n+1}}\frac{1}{Pr}\left(|f''|^s h'\right)'+\frac{2n+1}{4n+1}(fh)'=x\left(f'\frac{\partial h}{\partial x}-h'\frac{\partial f}{\partial x}\right) \tag{10.58}$$

The boundary and integral conditions (10.52) become

$$\left.\begin{array}{c} f=0,\quad f'=0 \\ h=1\quad\text{or}\quad h'=0 \\ f'\to 0,\quad h\to 0 \end{array}\right\}\quad\begin{array}{lll}\text{on} & \eta=0, & x\geqslant 0\\ & & \\ \text{as} & \eta\to\infty, & x\geqslant 0\end{array} \tag{10.59a}$$

$$\int_0^\infty f'h\,\mathrm{d}\eta = Q\,(n, Pr, x) \tag{10.59b}$$

It is apparent that Equations (10.57) and (10.58) permit similarity solutions if the exponent of $x$ in Equation (10.58) vanishes, i.e.

$$s = n - 1 \tag{10.60}$$

Under this condition, these equations reduce to the following ordinary differential equations:

$$\left(|f''|^{n-1} f''\right)' + \frac{2n+1}{4n+1} ff'' - \frac{n}{4n+1} f'^2 + h = 0 \tag{10.61}$$

$$\frac{1}{Pr}\left(|f''|^{n-1} h'\right)' + \frac{2n+1}{4n+1}(fh)' = 0 \tag{10.62}$$

which have to be solved subject to the boundary and integral conditions

$$\begin{gathered} f(0) = 0, \quad f'(0) = 0, \quad h(0) = 1 \quad \text{or} \quad h'(0) = 0 \\ f' \to 0, \quad h \to 0 \quad \text{as} \quad \eta \to \infty \end{gathered} \tag{10.63a}$$

$$\int_0^\infty f'h\,\mathrm{d}\eta = Q\,(n, Pr) \tag{10.63b}$$

It should be noted that for $n = 1$ (Newtonian fluids), Equations (10.61) and (10.62) reduce to those derived by Afzal (1980) and Ingham and Pop (1990). Further, the skin friction coefficient

$$C_f = 2Gr^{-\frac{1}{4n+1}} x^{-\frac{2n}{4n+1}} \left(\frac{\partial u}{\partial y}\right)_{y=0} \tag{10.64}$$

can be expressed as

$$C_f\,(Gr_x)^{\frac{1}{4n+1}} = 2\,|f''(0)|^n \tag{10.65}$$

if the variables (10.55) are used.

Equations (10.61) – (10.63) have been integrated numerically by Pop *et al.* (1993b) using the Runge-Kutta-Gill method for several values of $n$ and for $Pr = 0.72$, 10 and 100. For a Newtonian fluid ($n = 1$) the present results give for $C_f\,(Gr_x)^{\frac{1}{5}}$ the values 2.62012 for $Pr = 0.72$ and 1.85964 for $Pr = 6.7$, whilst the corresponding values obtained by Ingham and Pop (1990) are 2.6201 for $Pr = 0.72$ and 1.8596 for $Pr = 6.7$. This shows that the agreement between the two sets of results is excellent.

The results for various transport parameters, which are important for representing some heat transfer correlations are given in Tables 10.2 and 10.3 for the flow behaviour index $n$ ranging from 0.2 to 1.5 and for Prandtl numbers 10 and 100, respectively. It is noted from these tables that $f''(0)$ decreases as the values of $n$ and $Pr$ increase and this leads to a decrease in the skin friction coefficient as defined by

Table 10.2: *Numerical values of the computed parameters for* $Pr = 10$ *and the values* $0.2 \leqslant n \leqslant 1.5$.

| $n$ | $f''(0)$ | $f'_{\max}(\eta)$ | $f(\infty)$ | $Q$ |
|---|---|---|---|---|
| 0.2 | 3.21309 | 0.70945 | 3.46476 | 14.67177 |
| 0.4 | 1.56230 | 0.56938 | 2.48399 | 9.05100 |
| 0.6 | 1.08804 | 0.45349 | 1.52345 | 5.18968 |
| 0.8 | 0.95063 | 0.43117 | 1.32087 | 3.96055 |
| 1.0 | 0.86123 | 0.39276 | 0.99482 | 3.00209 |
| 1.2 | 0.90450 | 0.49054 | 1.62756 | 2.87300 |
| 1.5 | 0.82903 | 0.40676 | 0.70861 | 2.12471 |

Table 10.3: *Numerical values of the computed parameters for* $Pr = 100$ *and the values* $0.2 \leqslant n \leqslant 1.5$.

| $n$ | $f''(0)$ | $f'_{\max}(\eta)$ | $f(\infty)$ | $Q$ |
|---|---|---|---|---|
| 0.2 | 1.23283 | 0.22884 | 0.90717 | 3.33278 |
| 0.4 | 0.73858 | 0.20504 | 0.73486 | 2.33788 |
| 0.6 | 0.50828 | 0.13315 | 0.19407 | 1.04260 |
| 0.8 | 0.41895 | 0.09548 | 0.08289 | 0.53576 |
| 1.0 | 0.48062 | 0.12145 | 0.12585 | 0.52386 |
| 1.2 | 0.54364 | 0.16156 | 0.19320 | 0.48404 |
| 1.5 | 0.53094 | 0.13440 | 0.12537 | 0.31474 |

Equation (10.65). It is also seen that the parameter $I$, which serves to determine the reference temperature $T_{\text{ref}}$ through the Equation (10.56), decreases with an increase in $n$ and $Pr$.

Figures 10.6 and 10.7 display results for the fluid velocity and temperature profiles in the plume. It is seen from these figures that the maximum fluid velocity decreases with increasing values of the flow behaviour index $n$ and this maximum moves closer to the wall as the value of $n$ increases. We also see that the fluid velocity and the thermal boundary-layer thicknesses decrease as $n$ increases. Further, as the Prandtl number increases, the thinning effect of the thermal boundary-layer substantially affects the velocity boundary-layer region. Also, it can be noted from Figures 10.6(a) and 10.7(a) that for $n = 1$ the solution appears to intersect more curves for $Pr = 100$ than for $Pr = 10$. The reason for this appears to be the dependence of the Prandtl number on the index $n$, reference velocity $U_c$ and the reference length $l$ of the plate.

The important quantities in this flow geometry are the fluid velocity level, the surface temperature and the size of the boundary-layer region. As the flow proceeds downstream from a heated element which is located on an unheated part of the surface, it influences the cooling characteristics of any other element it may encounter.

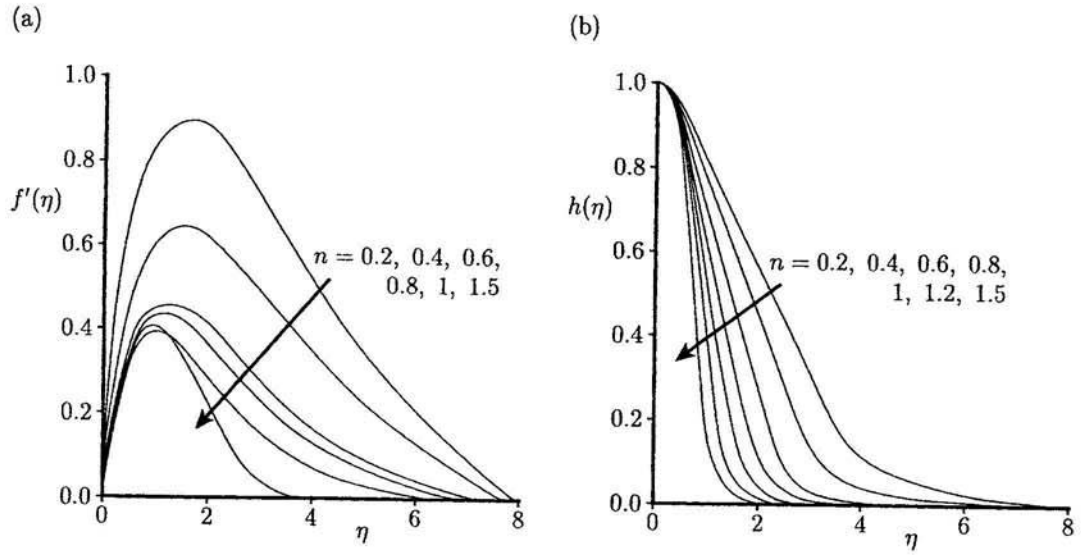


Figure 10.6: *(a) The fluid velocity, $f'(\eta)$, and (b) the temperature, $h(\eta)$, profiles for $Pr = 10$.*

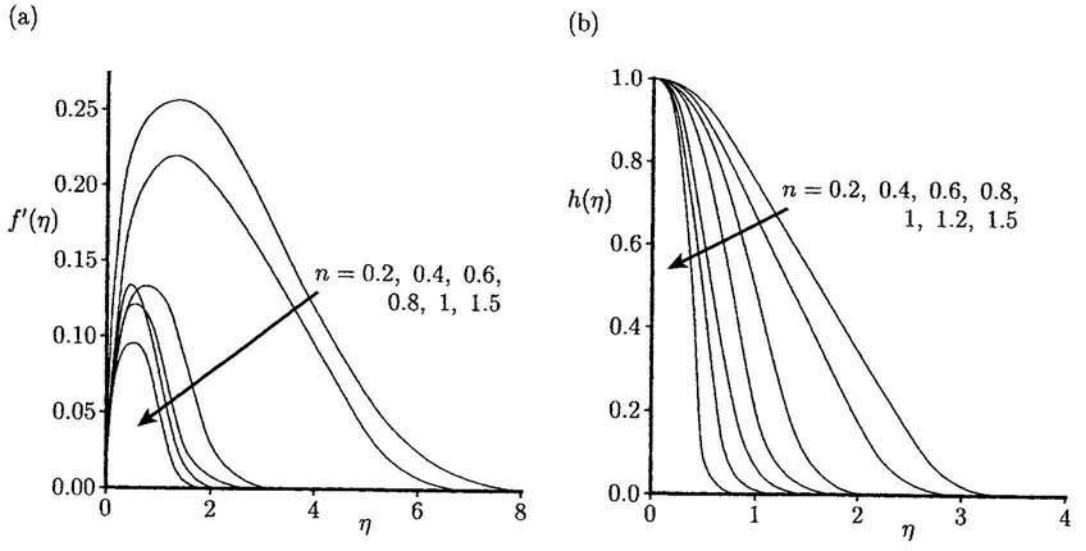


Figure 10.7: *(a) The fluid velocity, $f'(\eta)$, and (b) the temperature, $h(\eta)$, profiles for $Pr = 100$.*

An element downstream is immersed in a flowing heated fluid whose temperature and fluid velocity are determined by the distance between the two elements and the heat flux input $I$. The values of $f''(0)$, $f'_{\max}(\eta)$, $f(\infty)$ and $Q$, as given in Tables 10.2 and 10.3, allow the evaluation of the temperature and the fluid velocity fields at a downstream element.

## 10.5 Mixed convection boundary-layer flow from a horizontal circular cylinder and a sphere in non-Newtonian power-law fluids

Consider the mixed convection flow past a horizontal circular cylinder or a sphere of radius $a$ which are placed in a non-Newtonian power-law fluid of free stream velocity $U_\infty$ and temperature $T_\infty$, see Figure 10.8. We assume that the surface of the cylinder or sphere is kept at the uniform temperature $T_w$, where $T_w > T_\infty$ (heated surface) or $T_w < T_\infty$ (cooled surface). The analysis is also valid for downward flow and in this case the $x$-coordinate is measured from the upper stagnation point. Using the non-Newtonian power-law fluid model, the boundary-layer equations can be written as

$$\frac{\partial}{\partial x}\left(r^i u\right) + \frac{\partial}{\partial y}\left(r^i v\right) = 0 \tag{10.66}$$

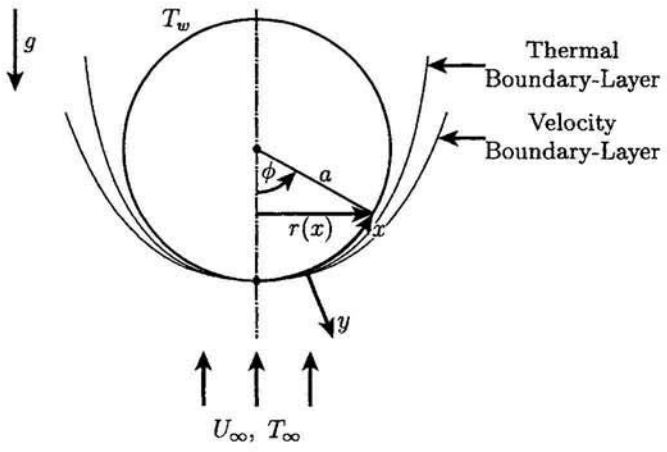


Figure 10.8: *Physical model and coordinate system.*

$$u\frac{\partial u}{\partial x}+v\frac{\partial u}{\partial y}=u_e\frac{\mathrm{d}u_e}{\mathrm{d}x}+\frac{\mu_0}{\rho}\frac{\partial}{\partial y}\left(\left|\frac{\partial u}{\partial y}\right|^{n-1}\frac{\partial u}{\partial y}\right)\pm g\beta\left(T-T_\infty\right)\sin\left(\frac{x}{a}\right) \tag{10.67}$$

$$u\frac{\partial T}{\partial x}+v\frac{\partial T}{\partial y}=\alpha_f\frac{\partial^2 T}{\partial y^2} \tag{10.68}$$

which have to be solved subject to the boundary conditions

$$\begin{array}{llll} u=0, \quad v=0, \quad T=T_w & \text{on} & y=0, & x\geqslant 0 \\ u\to u_e(x), \quad T\to T_\infty & \text{as} & y\to\infty, & x\geqslant 0 \end{array} \tag{10.69}$$

where $u_e(x)$ is the fluid velocity outside the boundary-layer, with $i=0$ for the cylinder and $i=1$ for the sphere, and the $\pm$ signs in Equation (10.67) correspond to assisting and opposing flows, respectively.

Equations (10.66) – (10.68), along with the boundary condition (10.69), were first solved numerically by Wang and Kleinstreuer (1988). They assumed that

$$\frac{u_e}{U_\infty}=0.92\left(\frac{x}{a}\right)-0.131\left(\frac{x}{a}\right)^3 \tag{10.70a}$$

for a cylinder in cross-flow and

$$\frac{u_e}{U_\infty}=1.5\left(\frac{x}{a}\right)-0.4371\left(\frac{x}{a}\right)^3+0.1481\left(\frac{x}{a}\right)^5-0.0423\left(\frac{x}{a}\right)^7 \tag{10.70b}$$

for a sphere and it was considered that both these equations hold for $0.5\leqslant n\leqslant 1.6$. In order to solve Equations (10.66) – (10.69) we introduce the following variables:

$$\begin{gathered} \xi=\tfrac{x}{a}, \quad \eta=\left(\tfrac{Re}{\xi}\right)^{\frac{1}{n+1}}\left(\tfrac{u_e}{U_\infty}\right)^{\frac{2-n}{1+n}}\tfrac{y}{a} \\ \psi=r(x)\left(\tfrac{\xi}{Re}\right)^{\frac{1}{n+1}}\left(\tfrac{u_e}{U_\infty}\right)^{\frac{1-2n}{1+n}}f(\xi,\eta), \quad \theta(\xi,\eta)=\tfrac{T-T_\infty}{|\Delta T|} \end{gathered} \tag{10.71}$$

where $r(x)$ is given by

$$r(x)=a\sin\left(\frac{x}{a}\right) \tag{10.72}$$

Using the transformation (10.71), Equations (10.66) – (10.68) take the following form:

$$\left(\left|f''\right|^{n-1}f''\right)'+A(\xi)ff''+\Pi(\xi)\left(1-f'^2\right)\pm\lambda B(\xi)\theta=\xi\left(f'\frac{\partial f'}{\partial\xi}-f''\frac{\partial f}{\partial\xi}\right) \tag{10.73}$$

$$\frac{C(\xi)}{Pr}\theta''+A(\xi)f\theta'=\xi\left(f'\frac{\partial\theta}{\partial\xi}-\theta'\frac{\partial f}{\partial\xi}\right) \tag{10.74}$$

and the boundary conditions (10.69) become

$$\begin{array}{llll} f=0, \quad f'=0, \quad \theta=1 & \text{on} & \eta=0, & \xi\geqslant 0 \\ f'\to 1, \quad \theta\to 0 & \text{as} & \eta\to\infty, & \xi\geqslant 0 \end{array} \tag{10.75}$$

The coefficients $A(\xi)$, $B(\xi)$, $C(\xi)$ and $\Pi(\xi)$ in Equations (10.73) and (10.74) are defined as follows:

$$A(\xi) = \begin{cases} \frac{1}{n+1} + \left(\frac{2n-1}{n+1}\right)\Pi(\xi) & \text{for the cylinder} \\ \frac{1}{n+1} + \left(\frac{2n-1}{n+1}\right)\Pi(\xi) + \frac{\xi}{r}\frac{\mathrm{d}r}{\mathrm{d}\xi} & \text{for the sphere} \end{cases}$$
$$B(\xi) = \frac{\xi \sin\xi}{\left(\frac{u_e}{U_\infty}\right)^2}, \quad C(\xi) = \left(\frac{u_e}{U_\infty}\right)^{\frac{3(1-n)}{n+1}} \xi^{\frac{n-1}{n+1}}, \quad \Pi(\xi) = \frac{\xi}{u_e}\frac{\mathrm{d}u_e}{\mathrm{d}\xi} \tag{10.76}$$

where the mixed convection parameter $\lambda$ is now given by

$$\lambda = \frac{Gr}{Re^{\frac{2}{2-n}}} \tag{10.77}$$

and $Gr$, $Re$ and $Pr$ are defined as follows:

$$Gr = \left(\frac{\mu_0}{\rho}\right)^{\frac{2}{n-2}} g\beta\,|\Delta T|\,a^{\frac{2+n}{2-n}}, \quad Re = \left(\frac{\rho}{\mu_0}\right) U_\infty^{2-n} a^n, \quad Pr = \frac{U_\infty a}{\alpha_f} Re^{-\frac{2}{n+1}} \tag{10.78}$$

Finally, the skin friction coefficient, $C_f$, and the local Nusselt number, $Nu$, are given by

$$C_f = \frac{2\tau_w}{\rho U_\infty^2}, \qquad Nu = \frac{a q_w}{k_f\,|\Delta T|} \tag{10.79}$$

and these can be expressed in the following form:

$$\begin{aligned} \frac{1}{2} C_f Re^{\frac{1}{n+1}} &= \xi^{-\frac{n}{n+1}} \left(\frac{u_e}{U_\infty}\right)^{\frac{3n}{n+1}} \left[f''(\xi,0)\right]^n \\ Nu Re^{-\frac{1}{n+1}} &= \xi^{-\frac{1}{n+1}} \left(\frac{u_e}{U_\infty}\right)^{\frac{2-n}{n+1}} \left[-\theta'(\xi,0)\right] \end{aligned} \tag{10.80}$$

Equations (10.73) and (10.74), subject to the boundary conditions (10.75), were solved numerically by Wang and Kleinstreuer (1988) for $n$ ranging from 0.52 to 1.6, $Pr = 10$ and 100, and $\lambda = 0$ (forced convection flow), 1 and 2 using the Keller-box method. Typical results for the skin friction coefficient and local Nusselt number are shown in Figures 10.9 to 10.12. It is observed from Figure 10.9(a) that for assisting flows pseudoplastic fluids ($n < 1$) generate higher, and dilatant fluids ($n > 1$) lower, skin frictions than Newtonian fluids ($n = 1$). However, both the power-law index $n$ and the buoyancy parameter $\lambda$ are less influential on the skin friction coefficient for a sphere than for horizontal cylinders, see Figure 10.9. Further, Figure 10.10(a) shows that, as expected, for a Newtonian fluid the local Nusselt number decreases monotonically along the surface of the cylinder. It reaches a maximum for pseudoplastic fluids and then, similar to Newtonian fluids, decreases

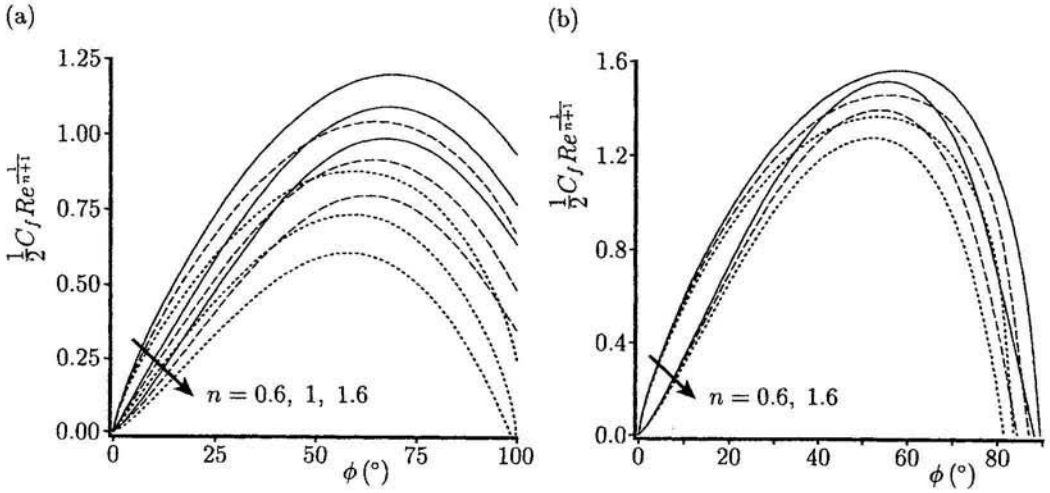


Figure 10.9: *Variation of the local skin friction coefficient with $\phi$ for $Pr = 100$ in the case of assisting flow for (a) a cylinder and (b) a sphere. The solutions for $\lambda = 0$ (forced convection), 1 and 2 are indicated by the dotted, broken and solid lines, respectively.*

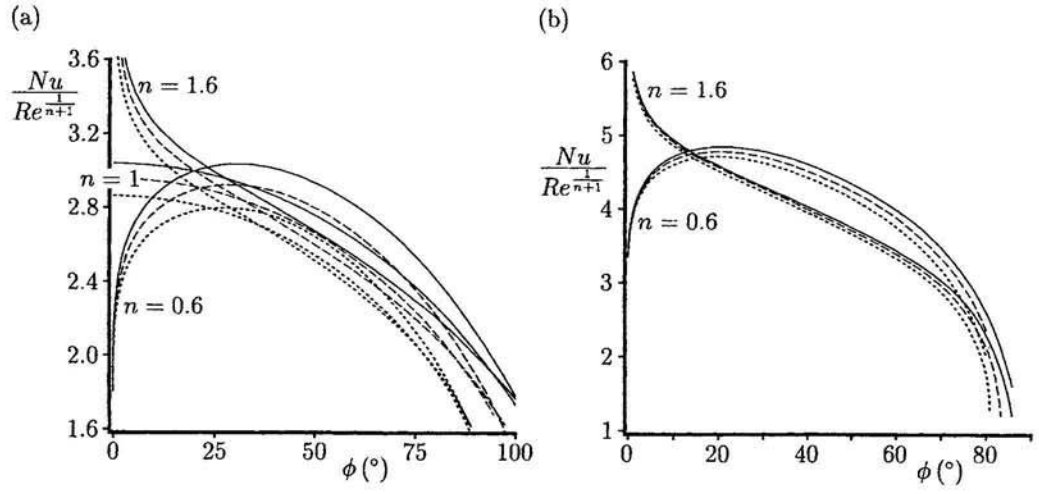


Figure 10.10: *Variation of the local Nusselt number with $\phi$ for $Pr = 100$ in the case of assisting flow for (a) a cylinder and (b) a sphere. The solutions for $\lambda = 0$ (forced convection), 1 and 2 are indicated by the dotted, broken and solid lines, respectively.*

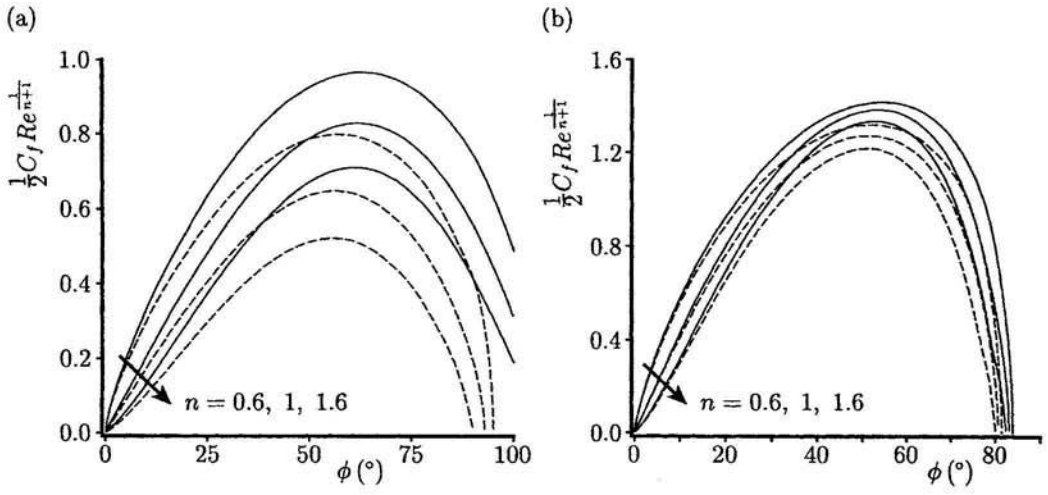


Figure 10.11: *Variation of the local skin friction coefficient with $\phi$ for $\lambda = 0.5$ and $Pr = 100$ in the cases of assisting flows (solid lines) and opposing flows (broken lines) for (a) a cylinder and (b) a sphere.*

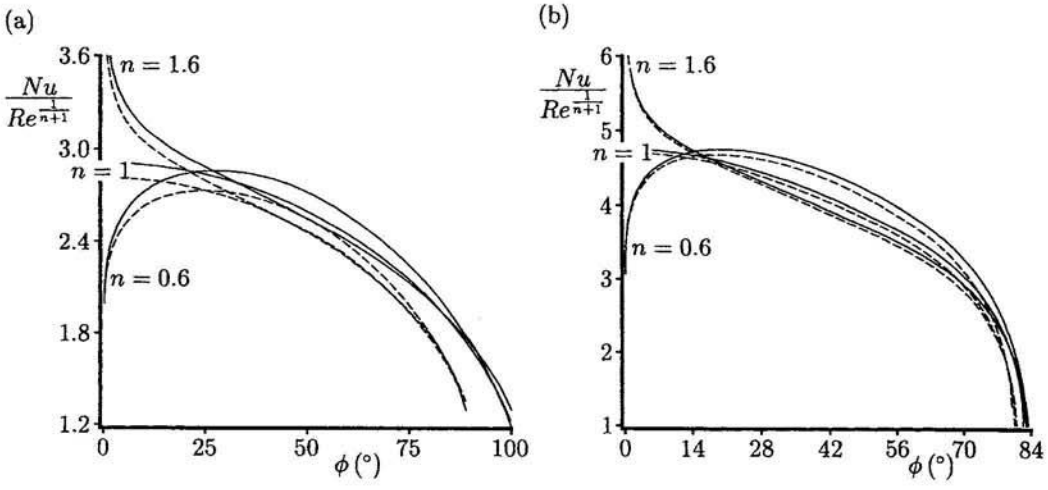


Figure 10.12: *Variation of the local Nusselt number with $\phi$ for $\lambda = 0.5$ and $Pr = 100$ in the cases of assisting flows (solid lines) and opposing flows (broken lines) for (a) a cylinder and (b) a sphere.*

gradually. In contrast, for dilatant fluids, the local Nusselt number reduces very rapidly in the vicinity of $\xi = 0$ (the forward stagnation point) and then follows, after a point of inflection, the general trend of the Newtonian fluids. This behaviour can be explained as follows. From Equation (10.80) we have

$$Nu\, Re^{-\frac{1}{n+1}} \sim \xi^{\frac{1-n}{1+n}} \left[-\theta'(\xi, 0)\right] \tag{10.81}$$

which implies that for $\xi \to 0$

$$Nu\, Re^{-\frac{1}{n+1}} \sim \begin{cases} 0 & \text{for} \quad n < 1 \\ \infty & \text{for} \quad n > 1 \end{cases} \tag{10.82}$$

provided that $\theta'(\xi, 0)$ is well behaved at the forward stagnation point.

On the other hand, Figures 10.11 and 10.12 show that for opposing flows the skin friction coefficient and the local Nusselt number have lower values than for assisting flows. This trend is comparable to the effect of lowering the buoyancy parameter $\lambda$, cf. Figures 10.9 and 10.10. In these cases, forced convection ($\lambda = 0$) is either retarded by the opposing buoyancy forces (cooled cylinder/sphere) or relatively less enhanced by decreasing the buoyancy forces (reduction of $\lambda$). As can be expected, the separation angle for opposing flows, see Figure 10.12, is similar to that of aiding flows.

## 10.6 Free convection boundary-layer flow of a micropolar fluid over a vertical flat plate

Convective flow over a flat plate which is immersed in a micropolar fluid has attracted an increasing amount of attention since the early studies of Eringen (1966, 1972). Results for this generic problem have been reported by several investigators, including Jena and Mathur (1982), Gorla and Takhar (1987), Yücel (1989), Gorla (1988, 1992), Gorla *et al.* (1990), Gorla and Nakamura (1993), Chiu and Chou (1993, 1994), Char and Chang (1995, 1997), Wang (1993, 1998), Hossain and Chaudhary (1998) and Rees and Pop (1998). These latter authors have shown, based on work by Rees and Bassom (1996) on the Blasius micropolar boundary-layer flow over a flat plate, that much more information about the solution of free convection boundary-layer flow of a micropolar fluid from a vertical flat plate can be found. A novel feature of these problems is that the boundary-layer develops a two-layer structure far from the leading edge, namely a mean layer and an inner, near-wall, layer. The near-wall layer is of constant thickness and it is the region where the microelements adjust from their natural free-stream orientation to that imposed by the presence of the solid boundary. It should be mentioned that the papers by Rees and Bassom (1996) and Rees and Pop (1998) are the most complete papers in the area of micropolar fluids and we shall therefore present here some results of these papers.

Consider a heated semi-infinite vertical flat plate with a constant wall temperature $T_w$, which is immersed in a micropolar fluid of temperature $T_\infty$, where $T_w > T_\infty$. The governing equations for the steady free convection flow of an incompressible micropolar fluid subject to the Boussinesq approximation can be written in the form, see Chiu and Chou (1993),

$$\frac{\partial \overline{u}}{\partial \overline{x}} + \frac{\partial \overline{v}}{\partial \overline{y}} = 0 \tag{10.83}$$

$$\rho\left(\overline{u}\frac{\partial \overline{u}}{\partial \overline{x}} + \overline{v}\frac{\partial \overline{u}}{\partial \overline{y}}\right) = -\frac{\partial \overline{p}}{\partial \overline{x}} + (\mu+\kappa)\left(\frac{\partial^2 \overline{u}}{\partial \overline{x}^2} + \frac{\partial^2 \overline{u}}{\partial \overline{y}^2}\right) + \kappa\frac{\partial \overline{N}}{\partial \overline{y}} + \rho g\beta\left(T - T_\infty\right) \tag{10.84}$$

$$\rho\left(\overline{u}\frac{\partial \overline{v}}{\partial \overline{x}} + \overline{v}\frac{\partial \overline{v}}{\partial \overline{y}}\right) = -\frac{\partial \overline{p}}{\partial \overline{y}} + (\mu+\kappa)\left(\frac{\partial^2 \overline{v}}{\partial \overline{x}^2} + \frac{\partial^2 \overline{v}}{\partial \overline{y}^2}\right) - \kappa\frac{\partial \overline{N}}{\partial \overline{x}} \tag{10.85}$$

$$\rho j\left(\overline{u}\frac{\partial \overline{N}}{\partial \overline{x}} + \overline{v}\frac{\partial \overline{N}}{\partial \overline{y}}\right) = -2\kappa\overline{N} + \kappa\left(\frac{\partial \overline{v}}{\partial \overline{x}} - \frac{\partial \overline{u}}{\partial \overline{y}}\right) + \gamma\left(\frac{\partial^2 \overline{N}}{\partial \overline{x}^2} + \frac{\partial^2 \overline{N}}{\partial \overline{y}^2}\right) \tag{10.86}$$

$$\overline{u}\frac{\partial T}{\partial \overline{x}} + \overline{v}\frac{\partial T}{\partial \overline{y}} = \alpha_f\left(\frac{\partial^2 T}{\partial \overline{x}^2} + \frac{\partial^2 T}{\partial \overline{y}^2}\right) \tag{10.87}$$

where $\overline{N}$ is the component of the microrotation vector normal to the $(\overline{x}, \overline{y})$-plane and $j$, $\kappa$ and $\gamma$ are the microinertia density, vortex viscosity and spin gradient viscosity, respectively. We assume that $\gamma$ is constant and is given by

$$\gamma = \left(\mu + \frac{\kappa}{2}\right) j \tag{10.88}$$

and this is invoked in order to allow the field equations to predict the correct behaviour in the limiting case when microstructure effects become negligible, and the microrotation, $\overline{N}$, reduces to the angular velocity, see Ahmadi (1976). The boundary conditions appropriate to Equations (10.83) – (10.87) are as follows:

$$\begin{aligned} &\overline{u} = 0, \quad \overline{v} = 0, \quad \overline{N} = -n\frac{\partial \overline{u}}{\partial \overline{y}}, \quad T = T_w \quad \text{on} \quad \overline{y} = 0, \quad \overline{x} \geqslant 0 \\ &\overline{u} \to 0, \quad \overline{v} \to 0, \quad \overline{N} \to 0, \quad T \to T_\infty \quad \text{as} \quad \overline{y} \to \infty, \quad \overline{x} \geqslant 0 \end{aligned} \tag{10.89}$$

where $n$ is a constant. On using Equation (10.86), and the boundary conditions (10.89), when $n = 0$ we obtain that $\overline{N} = 0$. This represents the case of concentrated particle flows in which the microelements close to the wall are not able to rotate. The case of $n = \frac{1}{2}$ results in the vanishing of the antisymmetric part of the stress tensor and represents weak concentration. Ahmadi (1976) suggested that in this case the particle spin is equal to fluid vorticity at the wall for fine particle suspensions. Then, the case of $n = 1$ is representative of turbulent boundary-layer flow, see Peddieson, Jr. (1972).

Next, we introduce the following non-dimensional variables

$$x = \frac{\overline{x}}{l}, \quad y = \frac{\overline{y}}{l}, \quad u = \frac{\overline{u}}{U_c}, \quad v = \frac{\overline{v}}{U_c}, \quad p = \frac{\overline{p} - p_\infty}{\rho U_c^2}, \quad \theta = \frac{T - T_\infty}{\Delta T}, \quad N = \frac{l\overline{N}}{U_c} \tag{10.90}$$

where $U_c = (g\beta\Delta T\, l)^{\frac{1}{2}}$ and we assume that the length scale is given by $j = l^2$. On using the expressions (10.90) in Equations (10.83) – (10.87), we obtain

$$\frac{\partial u}{\partial x} + \frac{\partial v}{\partial y} = 0 \tag{10.91}$$

$$u\frac{\partial u}{\partial x} + v\frac{\partial u}{\partial y} = -\frac{\partial p}{\partial x} + \frac{1+\mathcal{K}}{Gr^{\frac{1}{2}}}\left(\frac{\partial^2 u}{\partial x^2} + \frac{\partial^2 u}{\partial y^2}\right) + \theta + \frac{\mathcal{K}}{Gr^{\frac{1}{2}}}\frac{\partial N}{\partial y} \tag{10.92}$$

$$u\frac{\partial v}{\partial x} + v\frac{\partial v}{\partial y} = -\frac{\partial p}{\partial y} + \frac{1+\mathcal{K}}{Gr^{\frac{1}{2}}}\left(\frac{\partial^2 v}{\partial x^2} + \frac{\partial^2 v}{\partial y^2}\right) - \frac{\mathcal{K}}{Gr^{\frac{1}{2}}}\frac{\partial N}{\partial x} \tag{10.93}$$

$$u\frac{\partial N}{\partial x} + v\frac{\partial N}{\partial y} = -\frac{2\mathcal{K}}{Gr^{\frac{1}{2}}}N + \frac{\mathcal{K}}{Gr^{\frac{1}{2}}}\left(\frac{\partial v}{\partial x} - \frac{\partial u}{\partial y}\right) + \frac{1+\frac{1}{2}\mathcal{K}}{Gr^{\frac{1}{2}}}\left(\frac{\partial^2 N}{\partial x^2} + \frac{\partial^2 N}{\partial y^2}\right) \tag{10.94}$$

$$u\frac{\partial \theta}{\partial x} + v\frac{\partial \theta}{\partial y} = \frac{1}{Pr\, Gr^{\frac{1}{2}}}\left(\frac{\partial^2 \theta}{\partial x^2} + \frac{\partial^2 \theta}{\partial y^2}\right) \tag{10.95}$$

where $\mathcal{K} = \frac{\kappa}{\mu}$ is the micropolar parameter and $Pr$ and $Gr$ have been defined in the same way as for a standard Newtonian fluid; non-zero values of $\mathcal{K}$ cause coupling between the fluid flow and the microrotation component $N$.

We now invoke the boundary-layer approximation, namely

$$x = Gr\,\widehat{x}, \quad y = \widehat{y}, \quad u = Gr^{\frac{1}{2}}\frac{\partial \psi}{\partial y}, \quad v = -Gr^{\frac{1}{2}}\frac{\partial \psi}{\partial x}, \quad N = Gr^{\frac{1}{2}}\widehat{N} \tag{10.96}$$

which when substituted into Equations (10.91) – (10.95) and formally letting $Gr \to \infty$ leads to the following boundary-layer equations:

$$\frac{\partial \psi}{\partial \widehat{y}}\frac{\partial^2 \psi}{\partial \widehat{x}\partial \widehat{y}} - \frac{\partial \psi}{\partial \widehat{x}}\frac{\partial^2 \psi}{\partial \widehat{y}^2} = (1+\mathcal{K})\frac{\partial^3 \psi}{\partial \widehat{y}^3} + \theta + \mathcal{K}\frac{\partial \widehat{N}}{\partial \widehat{y}} \tag{10.97}$$

$$\frac{\partial \psi}{\partial \widehat{y}}\frac{\partial \widehat{N}}{\partial \widehat{x}} - \frac{\partial \psi}{\partial \widehat{x}}\frac{\partial \widehat{N}}{\partial \widehat{y}} = -\mathcal{K}\left(2\widehat{N} + \frac{\partial^2 \psi}{\partial \widehat{y}^2}\right) + \left(1 + \frac{1}{2}\mathcal{K}\right)\frac{\partial^2 \widehat{N}}{\partial \widehat{y}^2} \tag{10.98}$$

$$\frac{\partial \psi}{\partial \widehat{y}}\frac{\partial \theta}{\partial \widehat{x}} - \frac{\partial \psi}{\partial \widehat{x}}\frac{\partial \theta}{\partial \widehat{y}} = \frac{1}{Pr}\frac{\partial^2 \theta}{\partial \widehat{y}^2} \tag{10.99}$$

and the boundary conditions (10.89) become

$$\begin{aligned} &\psi = 0, \quad \tfrac{\partial \psi}{\partial \widehat{y}} = 0, \quad \widehat{N} = -n\tfrac{\partial^2 \psi}{\partial \widehat{y}^2}, \quad \theta = 1 \quad \text{on} \quad \widehat{y} = 0, \quad \widehat{x} \geqslant 0 \\ &\tfrac{\partial \psi}{\partial \widehat{y}} \to 0, \quad \widehat{N} \to 0, \quad \theta \to 0 \qquad\quad \text{as} \quad \widehat{y} \to \infty, \quad \widehat{x} \geqslant 0 \end{aligned} \tag{10.100}$$

As a prelude to obtaining numerical solutions, the governing Equations (10.97) – (10.99) and boundary conditions (10.100) are first transformed into a local non-similarity form. In order to do this we introduce the following variables:

$$\psi = X^{\frac{3}{2}} f(X,\eta), \quad \theta = g(X,\eta), \quad \widehat{N} = X^{\frac{1}{2}} h(X,\eta), \quad X = \widehat{x}^{\frac{1}{2}}, \quad \eta = \frac{\widehat{y}}{X^{\frac{1}{2}}} \tag{10.101}$$

where the functions $f$, $g$ and $h$ are given by the following set of partial differential equations

$$\begin{aligned}(1+\mathcal{K})\, f''' + \frac{3}{4} f f'' \\ -\frac{1}{2} f'^2 + \mathcal{K} h' + g = \frac{1}{2} X \left( f' \frac{\partial f'}{\partial X} - f'' \frac{\partial f}{\partial X} \right)\end{aligned} \tag{10.102}$$

$$\left(1 + \frac{1}{2}\mathcal{K}\right) h'' + \frac{3}{4} f h' - \frac{1}{4} h f' = \frac{1}{2} X \left( f' \frac{\partial h}{\partial X} - h' \frac{\partial f}{\partial X} \right) + \mathcal{K} X \left(2h + f''\right) \tag{10.103}$$

$$\frac{1}{Pr} g'' + \frac{3}{4} f g' = \frac{1}{2} X \left( f' \frac{\partial g}{\partial X} - g' \frac{\partial f}{\partial X} \right) \tag{10.104}$$

where primes denote differentiation with respect to $\eta$. The boundary conditions for these equations are given by

$$\begin{aligned} f = 0, \quad f' = 0, \quad h + n f'' = 0, \quad g = 1 \quad &\text{on} \quad \eta = 0, \quad X \geqslant 0 \\ f' \to 0, \quad h \to 0, \quad g \to 0 \quad &\text{as} \quad \eta \to \infty, \quad X \geqslant 0 \end{aligned} \tag{10.105}$$

At this stage we draw attention to the one case when Equations (10.102) – (10.105) reduce to a similarity form. The last term in Equation (10.103) may be regarded as the forcing term in this set of equations and if it were absent then it is possible for the resulting equations to have an $X$-independent solution. This one possibility for a similarity solution to exist is that the term $(2h + f'')$ is identically zero. However, it can easily be shown that even when $n = \frac{1}{2}$ then $h = -\frac{1}{2} f''$ does not give a consistent set of equations. Therefore, one cannot obtain a similarity solution in this way. The second possibility is that $\mathcal{K} = 0$ and in this case the Equation (10.103) is decoupled from the Equations (10.102) and (10.104). The resulting similarity solutions satisfy the following set of ordinary differential equations

$$f''' + \frac{3}{4} f f'' - \frac{1}{2} f'^2 + g = 0 \tag{10.106}$$

$$h'' + \frac{3}{4} f h' - \frac{1}{4} h f = 0 \tag{10.107}$$

$$\frac{1}{Pr} g'' + \frac{3}{4} f g' = 0 \tag{10.108}$$

which have to be solved subject to the boundary conditions

$$\begin{aligned} f(0) = 0, \quad f'(0) = 0, \quad h(0) + n f''(0) = 0, \quad g(0) = 1 \\ f' \to 0, \quad h \to 0, \quad g \to 0 \quad \text{as} \quad \eta \to \infty \end{aligned} \tag{10.109}$$

and hence the fluid flow and the temperature fields are unaffected by the microrotation of the fluid. It should be noted that Equations (10.106) and (10.108) represent the equations which govern the free convection boundary-layer flow of a Newtonian fluid over an isothermal vertical flat plate and are well known, see Section 1.3. On the other hand, Equation (10.107) has been solved numerically by Rees and Pop (1998) for $n = 1$ and when $Pr$ ranges from 0.1 to 10 and the profiles of the angular velocity $h$ are presented in Figure 10.13. As expected, these profiles remain negative and increase from the value $f''(0)$ to zero as $\eta$ increases from zero to infinity, see the boundary conditions (10.109). On the other hand, we can see from this figure that $h$ increases with the increase of $Pr$ for $0 \leqslant \eta \lesssim 2$ and decreases for $\eta \gtrsim 2$ when $Pr$ increases.

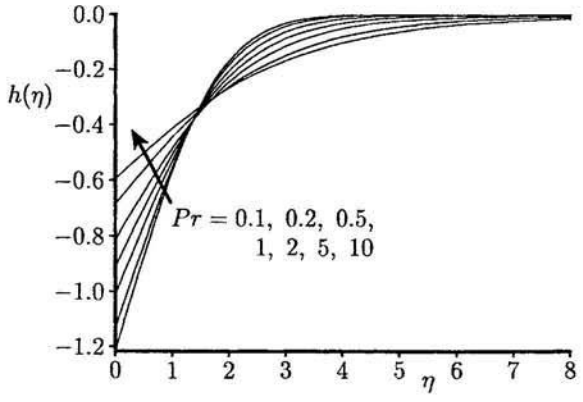


Figure 10.13: *Profiles, $h(\eta)$, of the reduced angular velocity for $\mathcal{K} = 0$ and $n = 1$.*

Further, the full boundary-layer equations were solved numerically by Rees and Pop (1998) using the Keller-box method and full details of the numerical procedure can be found in this paper. A selection of some of the numerical results for the non-dimensional skin friction, $f''(X, 0)$, and the rate of the wall heat transfer, $g'(X, 0)$, are presented (by full lines) in Figures 10.14 and 10.15, respectively, for $Pr = 6.7$ (water) and $\mathcal{K} = 0$, 0.25, 0.5, 0.75 and 1 for the respective cases $n = 0$, 0.5 and 1. It should be noted that all these curves are plotted against $X^{\frac{1}{2}}$ in order to more easily resolve the rapid variation near $X = 0$ (singularity) and the slow approach to the asymptotic solutions, which we will develop further.

Figure 10.14 shows that the curve corresponding to $\mathcal{K} = 0$ is a straight line, a result which is in accord with our earlier observation that $\mathcal{K} = 0$ represents the only similarity solution. When the micropolar parameter $\mathcal{K} \neq 0$ then the form of the skin friction variation depends very much on the values of $n$ and $\mathcal{K}$. It is always less than the $\mathcal{K} = 0$ value for sufficiently small values of $X$ but when $n = 0$ its

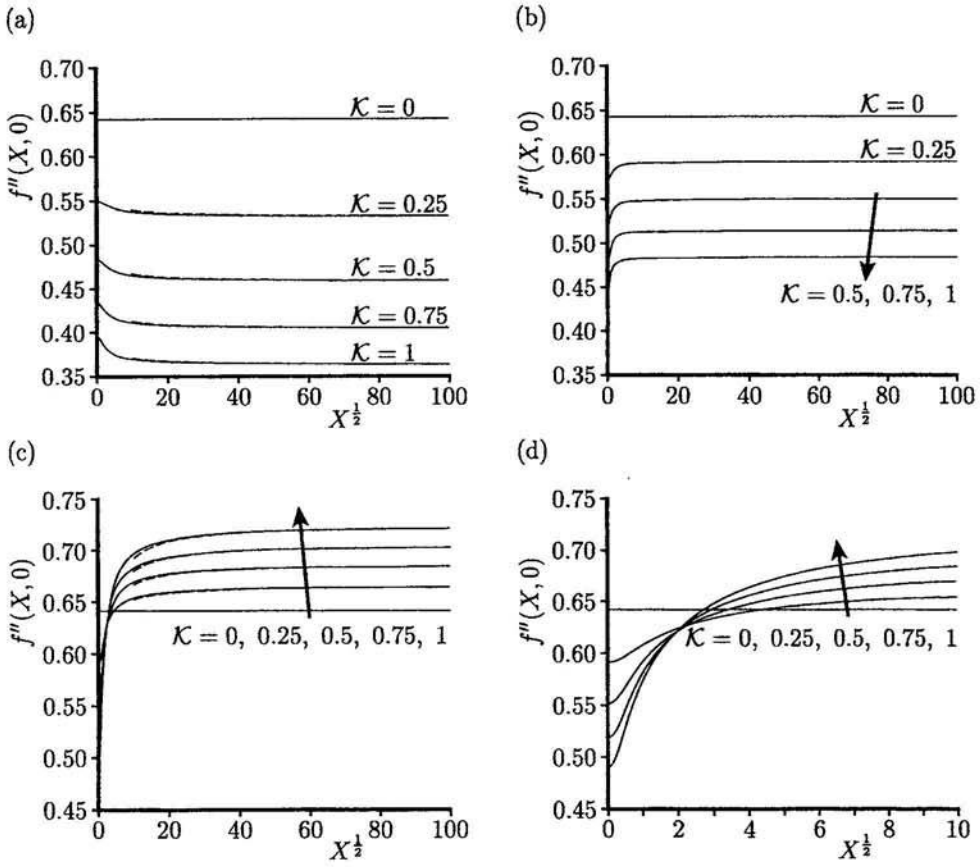


Figure 10.14: *Variation of the skin friction, $f''(X,0)$, with $X^{\frac{1}{2}}$ for $Pr = 6.7$ when (a) $n = 0$, (b) $n = 0.5$, (c) $n = 1$ and (d) a close-up view of (c) near $X = 0$. The numerical solutions are indicated by the solid lines and the asymptotic solutions (10.133a) for $n \neq \frac{1}{2}$ and (10.135a) for $n = \frac{1}{2}$ at large values of $X$ ($\gg 1$) are indicated by the broken lines.*

value decreases further as $X$ increases, whereas when $n = 1$ it eventually attains an asymptotic value above the $\mathcal{K} = 0$ result. However, for low values of $n$ the spread of the curves for different values of $\mathcal{K}$ is much greater than when $n = 1$.

The detailed evolution of the wall heat transfer shown in Figure 10.15 is a little more complicated than the skin friction curves. If we refer to the wall heat transfer in terms of its absolute value then the $\mathcal{K} \neq 0$ values are always less than the $\mathcal{K} = 0$ value and increase monotonically when $n = 0$, implying that the presence of the microstructure reduces the wall heat transfer. However, when $n = 1$ the variation is not monotonic; the wall heat transfer generally remains below the uniform $\mathcal{K} = 0$

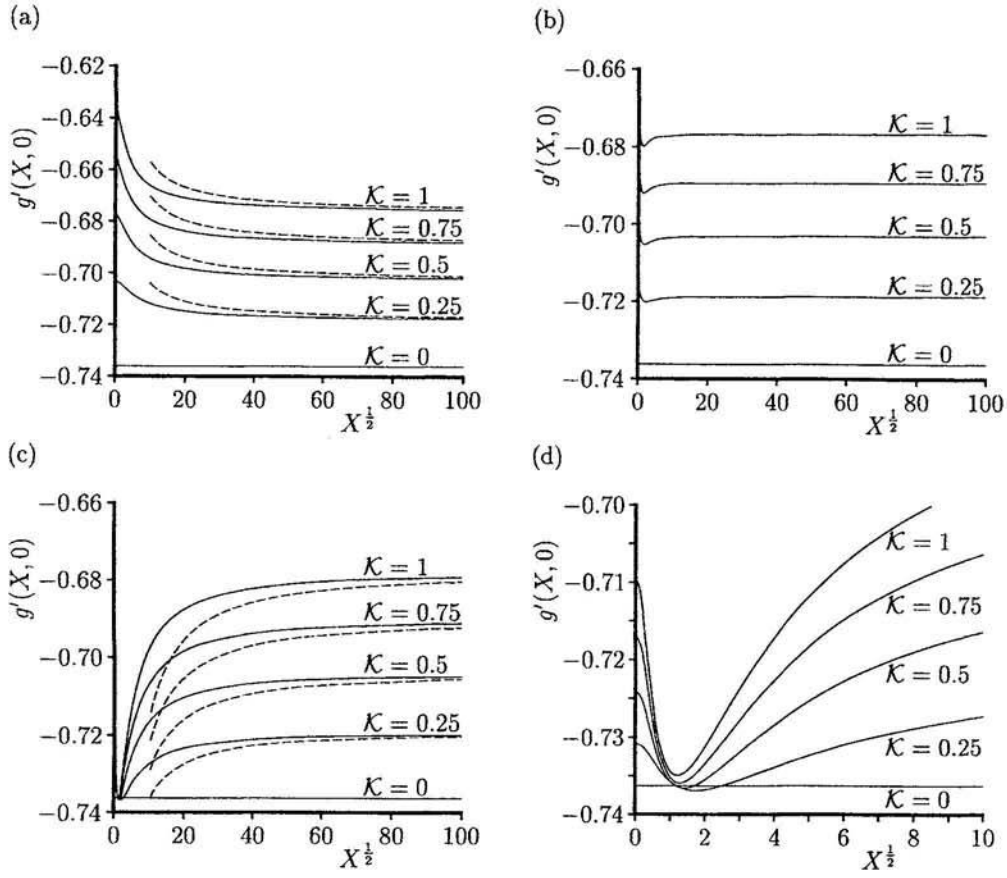


Figure 10.15: *Variation of the wall heat transfer, $g'(X,0)$, with $X^{\frac{1}{2}}$ for $Pr = 6.7$ when (a) $n = 0$, (b) $n = 0.5$, (c) $n = 1$ and (d) a close-up view of (c) near $X = 0$. The numerical solutions are indicated by the solid lines and the asymptotic solutions (10.133b) for $n \neq \frac{1}{2}$ and (10.135b) for $n = \frac{1}{2}$ at large values of $X$ ($\gg 1$) are indicated by the broken lines.*

value but can become slightly greater locally when $\mathcal{K}$ is sufficiently small. The variations of $f''(X,0)$ and $g'(X,0)$ for $Pr = 0.7$ (air) and the same values of the parameters $n$ and $\mathcal{K}$ can be found in the paper by Rees and Pop (1998). It was found that there is little qualitative difference between the results for water and for air, although the detailed quantitative results are quite different.

Figure 10.16 illustrates the contour plots of the function $\left(h + \frac{1}{2}f''\right)$ for the case $Pr = 0.7$, $n = 1$ and $\mathcal{K} = 1$. It shows the gradual development, as $X$ increases, of a thin, near-wall layer embedded within the main boundary-layer. Indeed, for the

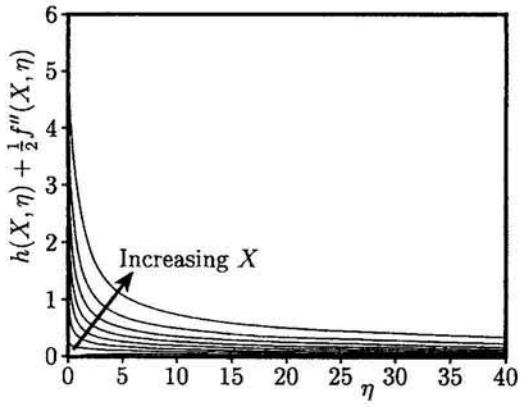


Figure 10.16: *Contour plots of the function* $\left(h(X,\eta) + \frac{1}{2}f''(X,\eta)\right)$ *for* $Pr = 0.7$, $\mathcal{K} = 1$ *and* $n = 1$.

micropolar Blasius boundary-layer flow, discussed by Rees and Bassom (1996), it was found that $\left(h + \frac{1}{2}f''\right) = 0$ when $n = \frac{1}{2}$, and that $\left(h + \frac{1}{2}f''\right) = 0$ except in a thin layer near to the flat plate when $n \neq \frac{1}{2}$. However, for the present problem, $h \neq -\frac{1}{2}f''$ even when $n = \frac{1}{2}$, but Figure 10.16 shows a similar development of a near-wall layer as $X$ increases. In order to examine this near-wall layer in more detail, for $\mathcal{K} \neq 0$, we make the substitution

$$\phi = h + \frac{1}{2}f'' \tag{10.110}$$

into Equations (10.102) – (10.104). Then we have

$$\left(1 + \frac{1}{2}\mathcal{K}\right) f''' + g + \mathcal{K}\phi' = \frac{1}{2}f'^2 - \frac{3}{4}ff'' + \frac{1}{2}X\left(f'\frac{\partial f'}{\partial X} - f''\frac{\partial f}{\partial X}\right) \tag{10.111}$$

$$(1 + \mathcal{K})\,\phi'' + \frac{1}{2}g' - 2\mathcal{K}X\phi = \frac{1}{4}\phi f' - \frac{3}{4}f\phi' + \frac{1}{2}X\left(f'\frac{\partial \phi}{\partial X} - \phi'\frac{\partial f}{\partial X}\right) \tag{10.112}$$

$$\frac{1}{Pr}g'' + \frac{3}{4}fg' = \frac{1}{2}X\left(f'\frac{\partial g}{\partial X} - g'\frac{\partial f}{\partial X}\right) \tag{10.113}$$

and the boundary condition (10.105) becomes

$$\begin{array}{lllllll} f = 0, & f' = 0, & \phi = \left(\frac{1}{2} - n\right) f'', & g = 1 & \text{on} & \eta = 0, & X \geqslant 0 \\ & f' \to 0, & \phi \to 0, & g \to 0 & \text{as} & \eta \to \infty, & X \geqslant 0 \end{array} \tag{10.114}$$

It is readily seen that for $X \gg 1$, the term $2\mathcal{K}X\phi$ from Equation (10.112) dominates this equation, unless $\phi$ is small, since $g'$ is $\mathbf{O}(1)$ as $X \to \infty$. Therefore, the

asymptotic forms of the solution of Equations (10.111) - (10.113), for $X \gg 1$, are given by

$$f \sim F_0(\eta), \quad g \sim G_0(\eta), \quad \phi \sim \frac{1}{4\mathcal{K}X} G_0'(\eta) \tag{10.115}$$

where $F_0$ and $G_0$ are given by the following ordinary differential equations

$$\left(1 + \frac{1}{2}\mathcal{K}\right) F_0''' + \frac{3}{4} F_0 F_0'' - \frac{1}{2} F_0'^2 + G_0 = 0 \tag{10.116}$$

$$\frac{1}{Pr} G_0'' + \frac{3}{4} F_0 G_0' = 0 \tag{10.117}$$

which have to be solved subject to the boundary conditions

$$\begin{array}{c} F_0(0) = 0, \quad F_0'(0) = 0, \quad G_0(0) = 1 \\ F_0' \to 0, \quad G_0 \to 0 \quad \text{as} \quad \eta \to \infty \end{array} \tag{10.118}$$

We note that Equations (10.116) - (10.118) can easily be written in terms of the classical vertical free convection equations using the transformation

$$F_0 = \left(1 + \frac{1}{2}\mathcal{K}\right)^{\frac{1}{2}} \widetilde{F}(\widetilde{\eta}), \quad G_0 = \widetilde{G}(\widetilde{\eta}), \quad \eta = \left(1 + \frac{1}{2}\mathcal{K}\right)^{\frac{1}{2}} \widetilde{\eta} \tag{10.119}$$

where $\widetilde{F}$ and $\widetilde{G}$ satisfy equations which are identical in form to Equations (10.106) and (10.108), but where the Prandtl number is replaced by $\left(1 + \frac{1}{2}\mathcal{K}\right) Pr$.

Further, it is seen from Equation (10.115) that the boundary conditions (10.114) for $\phi$ are not satisfied since the highest derivative in Equation (10.112) was neglected when forming the solution for $\phi$ in Equation (10.115), and hence this is a singular perturbation problem. Even without the numerical evidence presented earlier, it is clear that there must exist a thin layer, a near-wall layer, which is embedded within the main boundary-layer. However, it should be pointed out that the value of $n$ plays an important role in determining the size of $\phi$ in this near-wall layer. When $n = \frac{1}{2}$, we have $\phi = 0$ at $\eta = 0$, so that $\phi$ is $\mathbf{O}\left(X^{-1}\right)$ in order to match with the form given in Equation (10.115), but when $n \neq \frac{1}{2}$ the boundary conditions (10.114) for $\phi$ state that $\phi$ is $\mathbf{O}(1)$ at $\eta = 0$. Therefore these cases should be treated separately.

First, we introduce the near-wall layer variable $\zeta$ as follows:

$$\zeta = \eta X^{\frac{1}{2}} \tag{10.120}$$

which results from the balancing of the terms $2\mathcal{K}X\phi$ and $\phi''$ in Equation (10.112). It is worth pointing out that the comparison of the definition of $\zeta$ given by the Equation (10.120) with the definition of $\eta$ given in Equation (10.101), shows that $\zeta = \widehat{y}$, and therefore the near-wall layer has a constant thickness. Equations (10.111)

– (10.113) then become

$$\left(1+\frac{1}{2}\mathcal{K}\right)f'''+X^{-\frac{3}{2}}g+\mathcal{K}X^{-1}\phi'= X^{-\frac{1}{2}}\left(\frac{1}{2}f'^2-\frac{3}{4}ff''\right)+\frac{1}{2}X^{\frac{1}{2}}\left(f'\frac{\partial f'}{\partial X}-f''\frac{\partial f}{\partial X}\right) \tag{10.121}$$

$$(1+\mathcal{K})\,\phi''+\frac{1}{2}X^{-\frac{1}{2}}g'-2\mathcal{K}\phi= X^{-\frac{1}{2}}\left(\frac{1}{4}hf'-\frac{3}{4}fh'\right)+\frac{1}{2}X^{\frac{1}{2}}\left(f'\frac{\partial \phi}{\partial X}-\phi'\frac{\partial f}{\partial X}\right) \tag{10.122}$$

$$\frac{1}{Pr}g''+\frac{3}{4}X^{-\frac{1}{2}}fg'=\frac{1}{2}X^{\frac{1}{2}}\left(f'\frac{\partial g}{\partial X}-g'\frac{\partial f}{\partial X}\right) \tag{10.123}$$

where primes now denote differentiation with respect to $\zeta$. The boundary conditions appropriate to Equations (10.121) – (10.123) at $\zeta = 0$ are given by

$$f=0,\quad f'=0,\quad g=1,\quad \phi=\left(\frac{1}{2}-n\right)f'' \tag{10.124}$$

and the matching conditions as obtained from the small $\eta$ ($\ll 1$) limit of the main-layer solutions, are used to complete the specification of the boundary conditions. These matching conditions depend on whether or not $n=\frac{1}{2}$.

### 10.6.1 $n \neq \frac{1}{2}$

In this case the asymptotic solution of Equations (10.111) – (10.113) for $X \gg 1$ is sought in the following form:

$$\begin{aligned} f &= F_0(\eta)+X^{-\frac{1}{2}}F_1(\eta)+\ldots \\ g &= G_0(\eta)+X^{-\frac{1}{2}}G_1(\eta)+\ldots \\ \phi &= X^{-1}\Phi_0(\eta)+X^{-\frac{3}{2}}\Phi_1(\eta)+\ldots \end{aligned} \tag{10.125a}$$

in the main layer, and the asymptotic solution of Equations (10.121) – (10.123) has the form:

$$\begin{aligned} f &= X^{-1}f_0(\zeta)+X^{-\frac{3}{2}}f_1(\zeta)+\ldots \\ g &= 1+X^{-\frac{1}{2}}g_0(\zeta)+X^{-1}g_1(\zeta)+\ldots \\ \phi &= \phi_0(\zeta)+X^{-\frac{1}{2}}\phi_1(\zeta)+\ldots \end{aligned} \tag{10.125b}$$

in the near-wall layer. It should be noted that the equations and boundary conditions for $F_0$ and $G_0$ are precisely those given by Equations (10.116) – (10.118), while the functions $F_1$ and $G_1$ satisfy the following ordinary differential equations:

$$\left(1+\frac{1}{2}\mathcal{K}\right)F_1'''+G_1=\frac{3}{4}\left(F_0'F_1'-F_0F_1''\right)-\frac{1}{2}F_0''F_1 \tag{10.126}$$

$$\frac{1}{Pr}G_1''+\frac{3}{4}F_0G_1'+\frac{1}{4}F_0'G_1+\frac{1}{4}F_1G_0'=0 \tag{10.127}$$

which have to be solved subject to the boundary conditions

$$\begin{aligned} F_1(0) = 0, \quad G_1(0) = 0 \\ F_1' \to 0, \quad G_1 \to 0 \quad \text{as} \quad \eta \to \infty \end{aligned} \tag{10.128}$$

and the boundary condition for $F_1'(0)$ is obtained using the matching procedure. In order to do this, we observe that for $X \gg 1$ and $\eta \ll 1$, the functions $f$ and $g$ may be expanded as follows:

$$\begin{aligned} f &= F_0 + X^{-\frac{1}{2}} F_1 + \ldots \\ &= \left[\frac{1}{2}F_0''(0)\eta^2 + \frac{1}{6}F_0'''(0)\eta^3 + \ldots\right] + X^{-\frac{1}{2}}\left[F_1'(0)\eta + \frac{1}{2}F_1''(0)\eta^2 + \ldots\right] + \ldots \\ &= X^{-1}\left[\frac{1}{2}F_0''(0)\zeta^2 + F_1'(0)\zeta\right] + X^{-\frac{3}{2}}\left[\frac{1}{6}F_0'''(0)\zeta^3 + \frac{1}{2}F_1''(0)\zeta^2 + \ldots\right] + \ldots \end{aligned} \tag{10.129a}$$

$$\begin{aligned} g &= G_0 + X^{-\frac{1}{2}} G_1 + \ldots \\ &= \left[G_0'(0)\eta + \ldots\right] + X^{-\frac{1}{2}}\left[G_1'(0)\eta + \ldots\right] + \ldots \\ &= X^{-\frac{1}{2}}\left[G_0'(0)\zeta + \ldots\right] + X^{-1}\left[G_1'(0)\zeta + \ldots\right] + \ldots \end{aligned} \tag{10.129b}$$

and these expressions give the required large $\zeta$ ($\gg 1$) behaviour for the near-wall layer solution (10.125b).

Further, on substituting the series (10.125a) into Equations (10.121) – (10.123), we obtain a system of ordinary differential equations for the functions $f_0$, $f_1$, $g_0$, $g_1$, $\phi_0$ and $\phi_1$, which can easily be solved analytically, see Rees and Pop (1998). Hence, we have

$$\begin{aligned} f = X^{-1}\left[\frac{1}{2}F_0''(0)\zeta^2 - a_0 A_0 F_0''(0)\zeta + \ldots\right] \\ + X^{-\frac{3}{2}}\left[-\frac{1}{3(2+\mathcal{K})}\zeta^3 + \frac{1}{2}F_1''(0)\zeta^2 + \ldots\right] + \ldots \end{aligned} \tag{10.130}$$

for $\zeta \gg 1$, where

$$a_0 = \left(\frac{2\mathcal{K}}{1+\mathcal{K}}\right)^{\frac{1}{2}}, \qquad A_0 = \frac{\left(\frac{1}{2} - n\right)(1+\mathcal{K})}{2[1+\mathcal{K}(1-n)]} \tag{10.131}$$

On comparing expression (10.130) with Equation (10.129a) we obtain

$$F_1'(0) = -a_0 A_0 F_0''(0) \tag{10.132}$$

and therefore we now have all the boundary conditions in order to be able to solve Equations (10.126) and (10.127).

From these results we can now determine the skin friction and the wall heat transfer as follows:

$$\begin{aligned}\frac{\partial^2 f}{\partial \eta^2}(X,0) &= \left(\frac{\partial^2 f_0}{\partial \zeta^2} + X^{-\frac{1}{2}}\frac{\partial^2 f_1}{\partial \zeta^2} + \ldots\right)_{\zeta=0} \\ &= \frac{2+\mathcal{K}}{2\,(1+\mathcal{K}(1-n))}\left(F_0''(0) + X^{-\frac{1}{2}}F_1''(0) + \ldots\right)\end{aligned} \tag{10.133a}$$

$$\frac{\partial g}{\partial \eta}(X,0) = \left(\frac{\partial g_0}{\partial \zeta} + X^{-\frac{1}{2}}\frac{\partial g_1}{\partial \zeta} + \ldots\right)_{\zeta=0} = G_0'(0) + X^{-\frac{1}{2}}G_1'(0) + \ldots \tag{10.133b}$$

where the values of $F_0''(0)$, $G_0'(0)$, $F_1''(0)$ and $G_1'(0)$ are given in Table 10.4.

Table 10.4: *Variation of* $F_0''(0)$, $G_0'(0)$, $F_1''(0)$ *and* $G_1'(0)$ *with* $\mathcal{K}$ *for* $Pr = 6.7$.

| $\mathcal{K}$ | $F_0''(0)$ | $G_0'(0)$ | $F_1''(0)$ | $G_1'(0)$ |
|---|---|---|---|---|
| 0.00 | 0.64312 | −0.73597 | 0.65886 | 0.97683 |
| 0.25 | 0.59216 | −0.71827 | 0.58101 | 0.90901 |
| 0.50 | 0.54984 | −0.70265 | 0.51886 | 0.85253 |
| 0.75 | 0.51418 | −0.68868 | 0.46725 | 0.80107 |
| 1.00 | 0.48355 | −0.67608 | 0.42582 | 0.76234 |

The asymptotic solutions (10.133) are also included in Figures 10.14 and 10.15 (shown by broken lines). It can be seen that the agreement between the numerical (exact) and the asymptotic approximate solutions is very good.

### 10.6.2 $n = \frac{1}{2}$

It may be shown in this case that the appropriate expansions for $X \gg 1$ of $f$, $g$ and $\phi$ take the form

$$\begin{aligned} f &= F_0(\eta) + X^{-\frac{1}{2}}F_1(\eta) + X^{-1}F_2(\eta) + \ldots \\ g &= G_0(\eta) + X^{-\frac{1}{2}}G_1(\eta) + X^{-1}G_2(\eta) + \ldots \\ \phi &= X^{-1}\Phi_0(\eta) + X^{-\frac{3}{2}}\Phi_1(\eta) + X^{-2}\Phi_2(\eta) + \ldots \end{aligned} \tag{10.134a}$$

in the main layer, and

$$\begin{aligned} f &= X^{-1}f_0(\zeta) + X^{-\frac{3}{2}}f_1(\zeta) + X^{-2}f_2(\zeta) + \ldots \\ g &= 1 + X^{-\frac{1}{2}}g_0(\zeta) + X^{-1}g_1(\zeta) + X^{-\frac{3}{2}}g_2(\zeta) + \ldots \\ \phi &= X^{-1}\phi_0(\zeta) + X^{-\frac{3}{2}}\phi_1(\zeta) + X^{-2}\phi_2(\zeta) + \ldots \end{aligned} \tag{10.134b}$$

in the near-wall layer, where $F_0$, $G_0$ and $\phi_0$ are again given by Equations (10.116) – (10.118); $F_1 = G_1 = \phi_1 = 0$; and $F_2$, $G_2$ and $\phi_2$ are given by a system of ordinary differential equations, see Rees and Pop (1998).

Following the same procedure as that described previously for the $n \neq \frac{1}{2}$ case, it can be shown that the skin friction and the wall heat transfer are now given by

$$\frac{\partial^2 f}{\partial \eta^2}(X,0) = F_0''(0) + X^{-1}\left[F_2''(0) + \frac{G_0'(0)}{2(2+K)}\right] + \ldots \tag{10.135a}$$

$$\frac{\partial g}{\partial \eta}(X,0) = G_0'(0) + X^{-1}G_2'(0) + \ldots \tag{10.135b}$$

where the numerical values of $F_2''(0)$ and $G_2'(0)$ are given in the paper by Rees and Pop (1998).

Using these values then the asymptotic solution (10.135) for $n = \frac{1}{2}$ is also included in Figures 10.14 and 10.15 (shown by broken lines). We can see that the agreement of this asymptotic solution with the full numerical solution is very close and they are indistinguishable for $X \geqslant 100$.

## 10.7 Gravity-driven laminar film flow for non-Newtonian power-law fluids along a vertical wall

The theory of fluid flow in thin films has received considerable interest in recent years due to its importance in numerous technological applications. Examples of particular interest are in chemical engineering, where the mass or heat transfer associated with many falling film concepts such as coolers, evaporators and trickling filters are very important. This problem has attracted a great deal of interest from many investigators over the last three decades and much of the earlier work on this topic for both Newtonian and non-Newtonian fluids has been reviewed by Andersson and Irgens (1990), but recent contributions have been made by Pop *et al.* (1996c, 1997), Andersson and Shang (1998) and Shang and Andersson (1999). We shall present here some results developed by Andersson and Irgens (1988) for the steady laminar film flow of non-Newtonian power-law fluids down a vertical wall.

Consider the steady laminar film flow of non-Newtonian power-law fluids down a smooth vertical wall, see Figure 10.17, due to Andersson and Irgens (1988). According to this flow configuration the accelerating film can be divided into the following three distinct regions:

(i) the boundary-layer region, which consists of a developing viscous boundary-layer and an external free stream;

(ii) the fully viscous region, in which the boundary-layer extends to the film surface;

(iii) the region of developed flow, in which the streamwise gradients vanish.

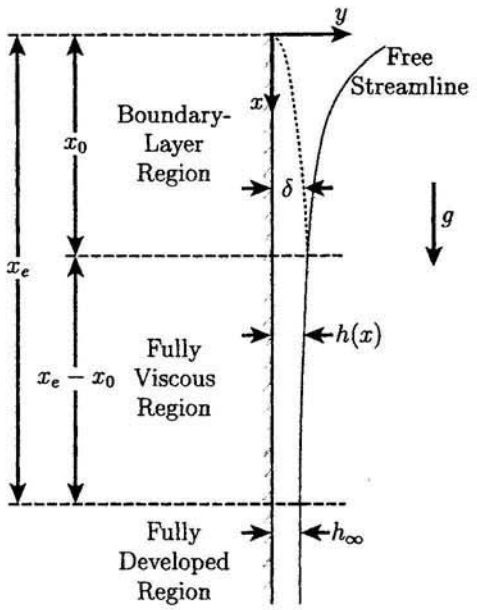


Figure 10.17: *Physical model and coordinate system.*

### 10.7.1 Boundary-layer region

In the boundary-layer region, the governing equation of the two-dimensional motion is, see Andersson and Irgens (1988), given by

$$u\frac{\partial u}{\partial x} + v\frac{\partial u}{\partial y} = u_e\frac{\mathrm{d}u_e}{\mathrm{d}x} + \frac{\mu_0}{\rho}\frac{\partial}{\partial y}\left(\left|\frac{\partial u}{\partial y}\right|^{n-1}\frac{\partial u}{\partial y}\right) \tag{10.136}$$

and this equation has to be solved subject to the boundary conditions

$$u = 0, \quad v = 0 \quad \text{on} \quad y = 0, \quad x \geqslant 0 \tag{10.137a}$$

$$u \to u_e(x) \quad \text{as} \quad y \to \delta(x), \quad x \geqslant 0 \tag{10.137b}$$

where the boundary-layer thickness $\delta(x)$ is smaller than the corresponding film thickness $h(x)$. The one-dimensional equation of motion for inviscid flow gives

$$u_e\frac{\mathrm{d}u_e}{\mathrm{d}x} = g \tag{10.138}$$

which on using the boundary condition that $u_e(x) = 0$ at the entrance $x = 0$, we obtain

$$u_e(x) = (2gx)^{\frac{1}{2}} \tag{10.139}$$

Next, we introduce the similarity variables

$$\psi = \left(\frac{1}{c_0 g}\frac{\mu_0}{\rho}u_e^{2n+1}\right)^{\frac{1}{n+1}} f(\eta), \qquad \eta = \left(c_0 g\left(\frac{\mu_0}{\rho}\right)^{-1} u_e^{-n}\right)^{\frac{1}{n+1}} y \tag{10.140}$$

where $c_0$ is a non-dimensional constant. Equation (10.136) then reduces to the following ordinary differential equation:

$$c_0 n\left|f''\right|^{n-1} f''' + \frac{2n+1}{n+1} f f'' + 1 - f'^2 = 0 \tag{10.141a}$$

and the boundary conditions (10.137) become

$$f(0) = 0, \quad f'(0) = 0, \quad f' \to 1 \quad \text{as} \quad \eta \to \infty \tag{10.141b}$$

It is worth noting that for $n = 1$ the problem defined by Equations (10.141) reduces to the corresponding Newtonian problem as studied by Andersson and Ytrehus (1985).

### 10.7.2 Fully developed flow region

In this region the viscous force due to the wall skin friction, namely

$$\tau_w = \mu_0\left|\frac{\partial u}{\partial y}\right|^{n-1}\frac{\partial u}{\partial y} \tag{10.142}$$

exactly balances the gravitational force. Therefore, after integration of the force-balance equation, Andersson and Irgens (1988) obtained

$$\frac{u(y)}{U_\infty} = \left(\frac{2n+1}{n+1}\right)\left[1 - \left(1 - \frac{y}{h_\infty}\right)^{\frac{n+1}{n}}\right] \tag{10.143}$$

where $h_\infty$ and $U_\infty$ are given by

$$h_\infty = \left[\frac{1}{g}\frac{\mu_0}{\rho}\left(\frac{2n+1}{n}Q\right)^n\right]^{\frac{1}{2n+1}}, \qquad U_\infty = \frac{Q}{h_\infty} = \left(\frac{1}{g}\frac{\mu_0}{\rho}\right)^{-\frac{1}{n}}\left(\frac{n}{2n+1}\right)h_\infty^{\frac{n+1}{n}} \tag{10.144}$$

with $Q$ being the total volumetric flow rate in the film.

### 10.7.3 Fully viscous flow region

In this region there is no external inviscid flow and the boundary-layer interacts directly with the free surface. Equation (10.136) applies throughout the film, but the boundary condition (10.137b) must be changed into a free surface condition. To

obtain the detailed flow behaviour in the fully viscous region one alternative is to use the integral form of Equation (10.136), namely

$$\frac{\mathrm{d}}{\mathrm{d}x}\int_0^{h(x)} u^2\,\mathrm{d}y = \frac{\mu_0}{\rho}\left[\left|\frac{\partial u}{\partial y}\right|^{n-1}\frac{\partial u}{\partial y}\right]_{y=0} + gh \tag{10.145}$$

and the appropriate boundary an integral conditions for this equation are as follows:

$$u(x,0) = 0, \qquad \left.\frac{\partial u}{\partial y}\right|_{y=h(x)} = 0 \tag{10.146a}$$

and

$$\int_0^{h(x)} u(x,y)\,\mathrm{d}y = Q \tag{10.146b}$$

Andersson and Irgens (1988) used the following fluid velocity profile

$$u(x,y) = \frac{Q}{h(x)}\left(1 + \frac{n}{n+1}\frac{h_\infty}{h(x)}\right)\left[1 - \left(1 - \frac{y}{h(x)}\right)^{\left(1+\frac{1}{n}\right)\frac{h(x)}{h_\infty}}\right] \tag{10.147}$$

which satisfies the boundary conditions (10.146a) and the continuity constraint (10.146b). On substituting Equation (10.147) into the Equation (10.145), leads to the following ordinary differential equation

$$\frac{\mathrm{d}\xi}{\mathrm{d}\zeta} = \frac{4\left(1+\frac{1}{n}\right)\zeta^{2n} + 8\left(1+\frac{1}{n}\right)\zeta^{2n-1} + 2\zeta^{2n-2}}{\left[2\left(1+\frac{1}{n}\right)\zeta + 1\right]^2\left\{\left[\left(1+\frac{1}{n}\right)\zeta + 1\right]^n - \left(2+\frac{1}{n}\right)^n\zeta^{2n+1}\right\}} \tag{10.148a}$$

which has to be solved subject to the boundary condition

$$\xi = \xi_0 \quad \text{on} \quad \zeta = \zeta_0 \tag{10.148b}$$

where $\xi$ and $\zeta$ are the non-dimensional streamwise coordinate and the local flow depth ratio which are defined as follows:

$$\xi = \frac{x}{h_\infty Re}, \qquad \zeta = \frac{h(x)}{h_\infty} \tag{10.149}$$

with $Re$ being the modified Reynolds number which is given by

$$Re = Q\left(\frac{\mu_0}{\rho}\right)^{-1}\left(\frac{h_\infty^2}{Q}\right)^{n-1} \tag{10.150}$$

The values $\xi_0$ and $\zeta_0$, which are the values of $\xi$ and $\zeta$ at $x = x_0$, are given by, see Andersson and Irgens (1988),

$$\begin{aligned} \xi_0 &= \tfrac{1}{2}\left[c_0^2\left(\tfrac{n}{2n+1}\right)^{n(2n-1)} f\left(\eta_\delta\right)^{-2(n+1)}\right]^{\frac{1}{2n+1}} \\ \zeta_0 &= \eta_\delta\, c_0^{-\frac{1}{n+1}}\left[2\left(\tfrac{2n+1}{n}\right)^{n-2}\xi_0\right]^{\frac{n}{2(n+1)}} \end{aligned} \tag{10.151}$$

where $\eta_\delta$ is the value of $\eta$ at the outer edge of the boundary-layer. Thus, the similarity fluid velocity profiles in the boundary-layer region can be written as

$$\frac{u(\xi_0,\eta)}{u(\infty,h_\infty)} = \frac{n+1}{2n+1}\left[2\left(\frac{2n+1}{n}\right)^n \xi_0\right]^{\frac{1}{2}} f'(\eta) \tag{10.152}$$

where the similarity fluid velocity profiles, $f'(\eta)$, were obtained by Andersson and Irgens (1988) by solving numerically Equation (10.141) for several values of $n$ with $c_0 = \frac{3}{2}$.

In Figure 10.18, the comparison between the similarity profiles (10.152) at $\xi = \xi_0$ (shown by different lines for $n = 0.5$, 1 and 1.5) and the asymptotic solution (10.143) (shown by circles) indicates the adaptation in the fluid velocity that must take place in the fully viscous region in Figure 10.17 before the film is fully developed at $x = x_E$. Further, Figure 10.18 shows that the similarity solution for the dilatant fluids ($n = 1.5$) at $x = x_0$ does not yet correspond to the fully developed flow conditions. The fluid velocities are lower than given by the asymptotic solution (10.143), and the liquid film must therefore be subject to a further acceleration downstream of the boundary-layer region. However, for the pseudoplastic fluids ($n = 0.5$), the velocity field at $x = x_0$ is rather undeveloped and a considerable amount of adaptation is required in order for it to reach the asymptotic solution.

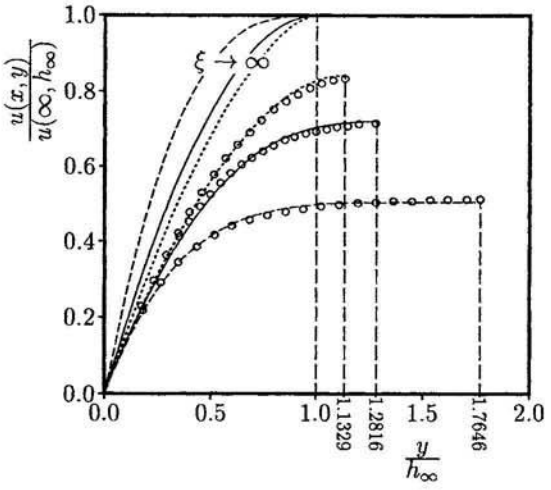


Figure 10.18: *Fluid velocity profiles at $\xi = \xi_0$, obtained from the similarity solution (10.152), and for $\xi \to \infty$. The solutions for $n = 0.5$, 1 and 1.5 are indicated by the broken, solid and dotted lines, respectively, and the asymptotic solution (10.143) at each value of $n$ is indicated by the symbols $\circ$.*

Further interesting results on this topic may be found in the recent publications by Andersson and Shang (1998) and Shang and Andersson (1999).